THE GEOLOGICAL SOCIETY OF AMERICA®

Searles Lake evaporite sequences: Indicators of late Pleistocene/Holocene lake temperatures, brine evolution, and pCO_2

Kristian J. Olson† and Tim K. Lowenstein
Department of Geological Sciences and Environmental Studies, Binghamton University, Binghamton, New York 13902-6000, USA

ABSTRACT

Searles Lake, California, was a saline-alkaline lake that deposited >25 non-clastic minerals that record the history of lake chemistry and regional climate. Here, the mineralogy and petrography from the late Pleistocene/Holocene (32–6 ka) portion of a new Searles Lake sediment core, SLAPP-SRLS17, is combined with thermodynamic models to determine the geochemical and paleoclimate conditions required to produce the observed mineral phases, sequences, and abundances. The models reveal that the primary precipitates formed by *open* system (i.e., fractional crystallization), whereas the early diagenetic salts formed by salinity-driven *closed* system back-reactions (i.e., equilibrium crystallization). For core SLAPP-SRLS17, the defining evaporite sequence trona → burkeite → halite indicates brine temperatures within a 20–29 °C range, implying thermally insulating lake depths >10 m during salt deposition. Evaporite phases reflect lake water pCO_2 consistent with contemporaneous atmospheric values of ~190–270 ppmv. However, anomalous layers of nahcolite and thenardite indicate pulses of pCO_2 > 700–800 ppm, likely due to variable CO_2 injection along faults.

Core sedimentology indicates that Searles Lake was continuously perennial between 32 ka and 6 ka such that evaporite units reflect periods of net evaporation but never complete desiccation. Model simulations indicate that cycles of partial evaporation and dilution strongly influence long-term brine evolution by amassing certain species, particularly Cl^-, that only occur in late-stage soluble salts. A model incorporating long-term brine dynamics corrects previous mass-balance anomalies and shows that the late Pleistocene/Holocene (32–6 ka) salts are partially inherited from the solutes introduced into earlier lakes going back at least 150 ka.

INTRODUCTION

Closed basin, non-marine halite [NaCl] deposits are commonly used to reconstruct hydroclimatic variability in arid environments including records of salinity (Du et al., 2019), temperature (Lowenstein et al., 1998; Roberts and Spencer, 1995), and lake level (Lowenstein et al., 1999; Kiro et al., 2017). Other evaporite minerals, such as sodium-bearing carbonates and sulfates, form at more specific temperatures and CO_2 concentrations than halite, which therefore make them potentially more sensitive paleoclimate indicators (Demicco and Lowenstein, 2020). Despite their proven applicability as paleoclimate proxies for temperature (Jagniecki et al., 2013; Wang et al., 2012), and atmospheric pCO_2 (Lowenstein and Demicco, 2006; Lowenstein et al., 2017; Jagniecki et al., 2015), Na-carbonate and Na-sulfate evaporites remain underutilized due to the scarcity of modern analog studies and the challenges associated with modeling complex multicomponent brines.

Searles Lake, California, (Fig. 1) was a Pleistocene-Holocene saline-alkaline lake that deposited a suite of >25 non-clastic minerals (Table 1; Smith and Haines, 1964; Smith, 1979), which makes it an ideal candidate for exploring the paleoclimatic and paleoenvironmental controls on multiphase evaporite deposition. Studies characterizing the mineralogy, areal distribution, and masses of Searles Lake evaporites indicated that specific evaporite mineral assemblages and masses vary stratigraphically at both unit and multi-unit scales (Smith, 1979). Such stratigraphic variations suggest that long-term brine evolution was moderated by shorter duration paleoenvironmental and paleoclimatic rhythms. Here, thermodynamic model codes are used to simulate the evaporation of the presumed source water for Searles Lake, the Owens River, over a range of temperatures and CO_2 concentrations. The mineral sequences found in a new Searles Lake sediment core, SLAPP-SRLS17, are then compared to evaporation models to interpret paleoclimate signals (temperature, pCO_2) and brine evolution in the Searles Basin from ca. 32–6 ka.

GEOLOGIC BACKGROUND

Owens River System and Chemistry

The modern Owens River is fed by runoff from the eastern flank of the Sierra Nevada and flows from the Long Valley Caldera in the northern watershed south to its modern terminus at Owens Lake (Fig. 1). During pluvial conditions, the ancestral Owens River was the link in a chain of five lakes formed by successive downstream spillover: Owens Lake spilled into China Lake, which then spilled into Searles Lake; at high lake levels, Searles Lake coalesced with China Lake and spilled into Panamint Lake (aka Gale Lake); lastly, Panamint Lake overflowed and spilled into Lake Manly in Death Valley (Fig. 1, inset) (Gale, 1914; Smith, 1979). Searles Lake likely overflowed during Marine Isotope Stages 2 and 6 but was otherwise the main terminus for the Owens River throughout much of the late Pleistocene (Smith, 2009).

The solutes delivered to Searles Lake via the ancestral Owens River (Table 2) are derived from two principal sources: (1) low-temperature weathering of Sierra Nevada granitoids (mainly plagioclase feldspar) and (2) hydrothermal spring discharge associated with the Long Valley Caldera (Fig. 1). Hot Creek is the Owens River tributary flowing from Long Valley Caldera (Fig. 1, inset), which accounts for 35% of the total dissolved solids (TDS) of modern Owens River water, supplies its bulk chlorinity and total alkalinity (i.e., sum of all dissolved species of carbonate) (Table 2), and is the likely source of boron, fluoride, and lithium to Searles Lake (Smith, 1976). The Hot Creek hydrothermal waters are so essential to the chemical signature of Searles Lake that the mineral facies of the Searles Lake deposit have been used to determine when magmatism began in the Long Valley Caldera (Lowenstein et al., 2016). Nonetheless, the degree to which modern Owens River chemistry is an accurate analog to its ancestral counterpart is unclear. Pine Creek, which

†kolson2@binghamton.edu.

GSA Bulletin; https://doi.org/10.1130/B35857.1; 9 figures; 4 tables.

For permission to copy, contact editing@geosociety.org
© 2021 Geological Society of America

Downloaded from http://pubs.geoscienceworld.org/gsa/gsabulletin/article-pdf/doi/10.1130/B35857.1/5242712/b35857.pdf
by SUNY Binghamton Science Library user

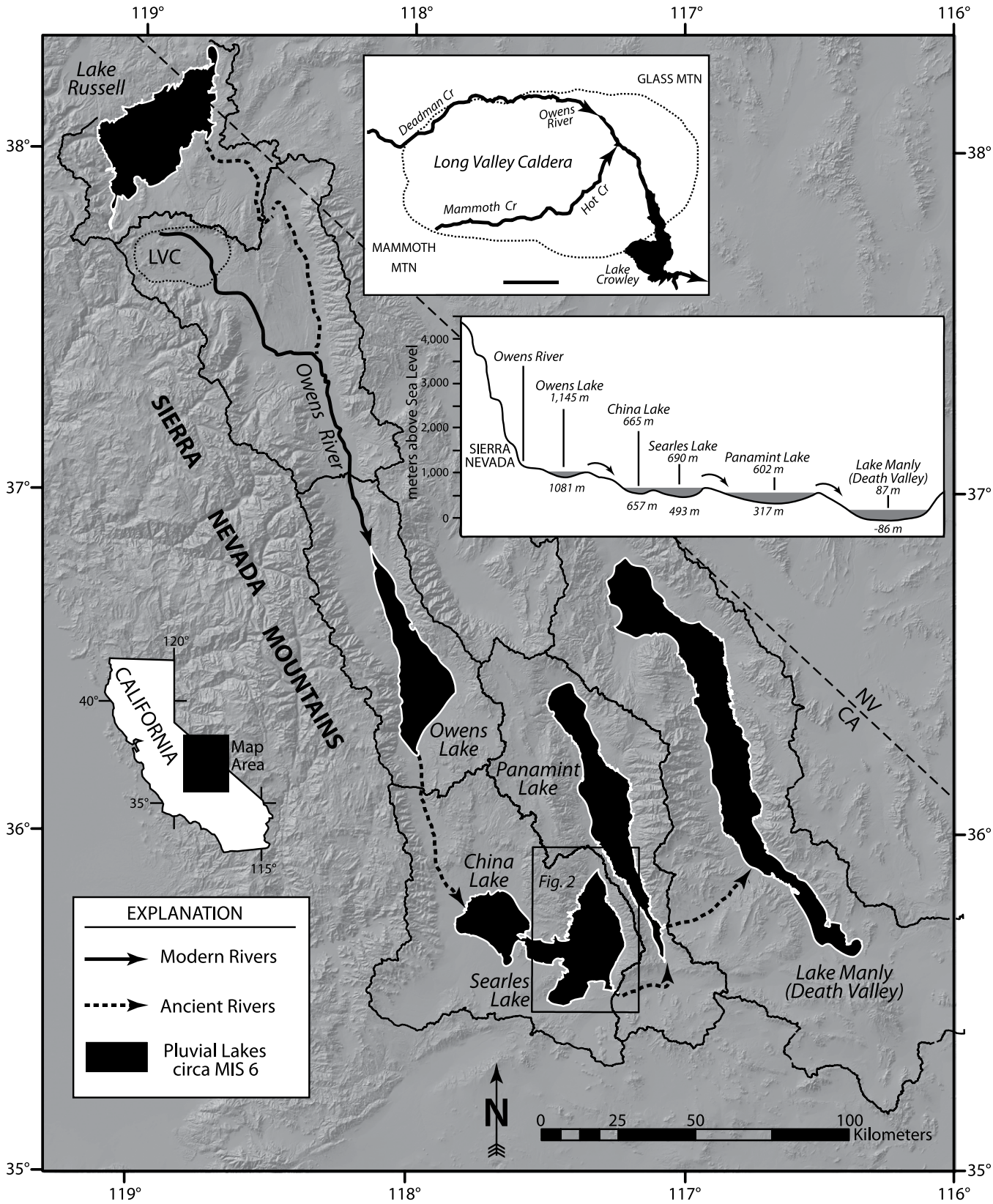

Figure 1. Regional map shows modern rivers and lakes/playas and the maximum extent of their pluvial counterparts ca. Marine Isotope Stage (MIS) 6. Inset elevations are shown for modern basin floor and sill/high shoreline. Modified from Smith (1979); Sorey (1985); and Rosenthal et al. (2017).

Downloaded from http://pubs.geoscienceworld.org/gsa/gsabulletin/article-pdf/doi/10.1130/B35857.1/5242712/b35857.pdf
by SUNY Binghamton Science Library user

TABLE 1. CHEMICAL FORMULAS OF MINERALS DISCUSSED

Mineral	Formula
Aphthitalite	$(K,Na)_3Na(SO_4)_2$
Aragonite	$CaCO_3$
Borax	$Na_2(B_4O_5)(OH)_4 \cdot 8H_2O$
Burkeite*	$Na_6(CO_3)(SO_4)_2$
Calcite	$CaCO_3$
Dolomite	$CaMg(CO_3)_2$
Gaylussite	$Na_2Ca(CO_3)_2 \cdot 5H_2O$
Halite	NaCl
Hanksite*	$Na_{22}K(SO_4)_9(CO_3)_2Cl$
Mirabilite	$Na_2SO_4 \cdot 10H_2O$
Nahcolite	$NaHCO_3$
Natron	$Na_2CO_3 \cdot 10H_2O$
Northupite*	$Na_3Mg(CO_3)_2Cl$
Pirssonite*	$Na_2Ca(CO_3)_2 \cdot 2H_2O$
Thenardite	Na_2SO_4
Trona	$Na_2CO_3 \cdot NaHCO_3 \cdot 2H_2O$

Note: For a complete list of Searles Lake minerals see Smith and Haines (1964) and Smith et al. (1983).
*Minerals first described at Searles Lake.

supplies 39% of the TDS of modern Owens River water, has an anomalously high SO_4^{2-} concentration (Table 2) likely due to sulfide mineralization associated with tungsten mining in the Pine Creek watershed (Pretti and Stewart, 2002). Modern Owens River water may therefore be enriched in SO_4^{2-} relative to its ancestral composition, while alkalinity and Cl^- concentrations would likely vary in concert with the hydrothermal activity of Long Valley Caldera.

Searles Lake Evaporites

The earliest lacustrine sediments in Searles Basin are inferred from paleomagnetic dates to have formed ca. 3.18 m.y. ago, with evaporite precipitation beginning ca. 2.0 m.y. ago (Smith et al., 1983). At its highest known levels (Marine Oxygen Isotope Stages 2 and 6), Searles Lake had a surface area of ~1000 km^2 and was >200 m deep (Smith, 2009). Today, Searles Lake is a 100 km^2 dry salt pan with large-scale economic mineral extraction from subsurface brines (Fig. 2A). Fluctuations in inflow and evaporation rates during the Pleistocene and Holocene are loosely characterized by the alternating deposits of salts and muds in Searles Lake deposits (Fig. 2B). The subsurface stratigraphy is divided by lithology into the Overburden Mud (6–0 ka), Upper Salt (10–6 ka), Parting Mud (24–10 ka), Lower Salt (32–24 ka), Bottom Mud (130–32 ka), and Mixed Layer (3.18–0.13 Ma) (Table 3) (Smith, 1979; Smith et al., 1983). The Lower Salt is further divided into seven salt units (S1–S7) and six mud units (M2–M7) (Fig. 2B) (Smith, 1962). Searles Lake chemical sediments include carbonates, sulfates, borates, silicates, and chlorides, which are highly variable in their stratigraphic distribution (Table 3). Generally, the chemical sediments of Searles Lake can be divided into three genetic types based on their timing of formation: (1) "early" insoluble alkaline earth carbonates, (2) primary bedded evaporites, and (3) "later" diagenetic salts.

Brine Evolution

The depositional history of Searles Lake evaporites is related to how the chemical composition and salinity of the brine evolved through time. The chemistry of evaporating lake water changes as mineral precipitation fractionally removes certain ions while others increase in concentration. Brine evolution is dependent on mineral solubility, which is governed by *K*, the equilibrium constant, and the activities of all species in the water. Brine evolution is strongly influenced by precipitation of the early, relatively insoluble minerals such as calcite [$CaCO_3$] and gypsum [$CaSO_4 \cdot 2H_2O$] according to the *principle of chemical divides* (Fig. 3) (Hardie and Eugster, 1970). Calcite, as the least soluble salt to form in most natural waters, is the first precipitate during evaporation. If $Ca^{2+} > CO_3^{2-}$, then carbonate is almost completely consumed during calcite precipitation. The relative proportion of Ca^{2+} to SO_4^{2-} after calcite precipitation then dictates the chemical evolution of the water during gypsum precipitation. If $SO_4^{2-} > Ca^{2+}$, then the water evolves to a Mg-SO_4-Na-K-Cl brine (e.g., seawater) following gypsum formation. If $Ca^{2+} > SO_4^{2-}$, then the solution evolves to a Ca-Na-Mg-K-Cl brine (e.g., the Dead Sea). The Owens River contains three times as much alkalinity as Ca^{2+} (Table 2), and therefore calcite precipitation exhausts most of the Ca^{2+} and the water evolves to a Na-HCO_3-CO_3-Mg-K-Cl_SO_4 brine.

The physicochemical behavior of high ionic-strength solutions is more complex than that of dilute solutions because interactions between ions, and between ions and H_2O, produce "non-ideal" behavior and divergence of ionic *concentration* and ionic *activity* (Pitzer, 1973). Early attempts to reproduce the Searles Lake evaporite sequences relied on graphical phase equilibria relations, which provided *relative* aH_2O and pCO_2 mineral precipitation dependencies (Eugster and Smith, 1965). Following the development of Pitzer's ion interaction model, computer programs were developed to calculate activity coefficients and mineral solubilities for concentrated brines (Harvie and Weare, 1980; Harvie et al., 1984).

Pitzer-based programs have since been applied to Searles Lake evaporites to derive characteristic salts from Owens River water (Felmy and Weare, 1986; Lowenstein et al., 2016) and constrain hydroclimate variability (Janick and Demicco, 2019). However, those studies maintained constant temperature and pCO_2 conditions during model runs, which likely accounts for inconsistencies between their modeled and observed mineral records (Felmy and Weare, 1986). Demicco and Lowenstein (2020) demonstrated that subtle variations in paleoenvironmental conditions, such as lake temperature and pCO_2, will produce predictable changes in evaporite mineralogy and abundance. Here, the Pitzer-based code EQL/EVP (equilibrium program/evaporation program) (Risacher and Clement, 2001) is used to model various brine evolution pathways for Owens River water to constrain the paleoclimate conditions required to reproduce the observed mineralogical sequence of the late Pleistocene Lower Salt and Parting Mud and Holocene Upper Salt at Searles Lake.

TABLE 2. CHEMISTRY OF MODERN OWENS RIVER WATER AND IMPORTANT TRIBUTARIES

Component*	Owens River 1974–1985†					Important tributaries§	
	Mean	Min	Max	*n*	Stdev	Hot Creek	Pine Creek
Discharge	13.49	0.14	26.9	766	5.66	2.1	3.5
pH	8.1	7.1	9.6	109	0.50	6.7	7.4
Alk	1.99	0.78	2.80	89	0.40	2.72	0.57
Cl	0.37	0.12	0.71	102	0.12	0.94	0.05
SO_4	0.24	0.05	0.48	100	0.08	0.22	1.32
Na	1.39	0.24	2.35	101	0.36	2.83	2.31
K	0.10	0.05	0.15	102	0.02	0.20	0.04
Ca	0.54	0.02	0.80	102	0.10	0.34	0.49
Mg	0.16	0.37	0.26	101	0.04	0.28	0.05
B	0.07#	N.D.	N.D.	N.D.	N.D.	N.D.	N.D.
Alk/Cl	5.44	N.A.	N.A.	N.A.	N.A.	2.89	12.04
Na/Cl	3.78	N.A.	N.A.	N.A.	N.A.	3.01	49.23
SO_4/Cl	0.64	N.A.	N.A.	N.A.	N.A.	0.23	28.00
Ca/Cl	1.47	N.A.	N.A.	N.A.	N.A.	0.36	10.45
Mg/Cl	0.45	N.A.	N.A.	N.A.	N.A.	0.30	0.96
K/Cl	0.27	N.A.	N.A.	N.A.	N.A.	0.21	0.91

*Discharge in m^3/s; ionic concentrations in mmol/kg H_2O.
†Hollett et al. (1991).
§Pretti and Stewart (2002).
#Smith (1976).

MATERIALS AND METHODS

Core SLAPP-SRLS17

Sonic drilling was used to recover sediment cores from Searles Lake in January 2017. Core SLAPP-SRLS17-1A (35.737153191, −117.330298425), drilled to 76.7 m below surface (mbs), records ca. 130 k.y. of continuous

Downloaded from http://pubs.geoscienceworld.org/gsa/gsabulletin/article-pdf/doi/10.1130/B35857.1/5242712/b35857.pdf
by SUNY Binghamton Science Library user

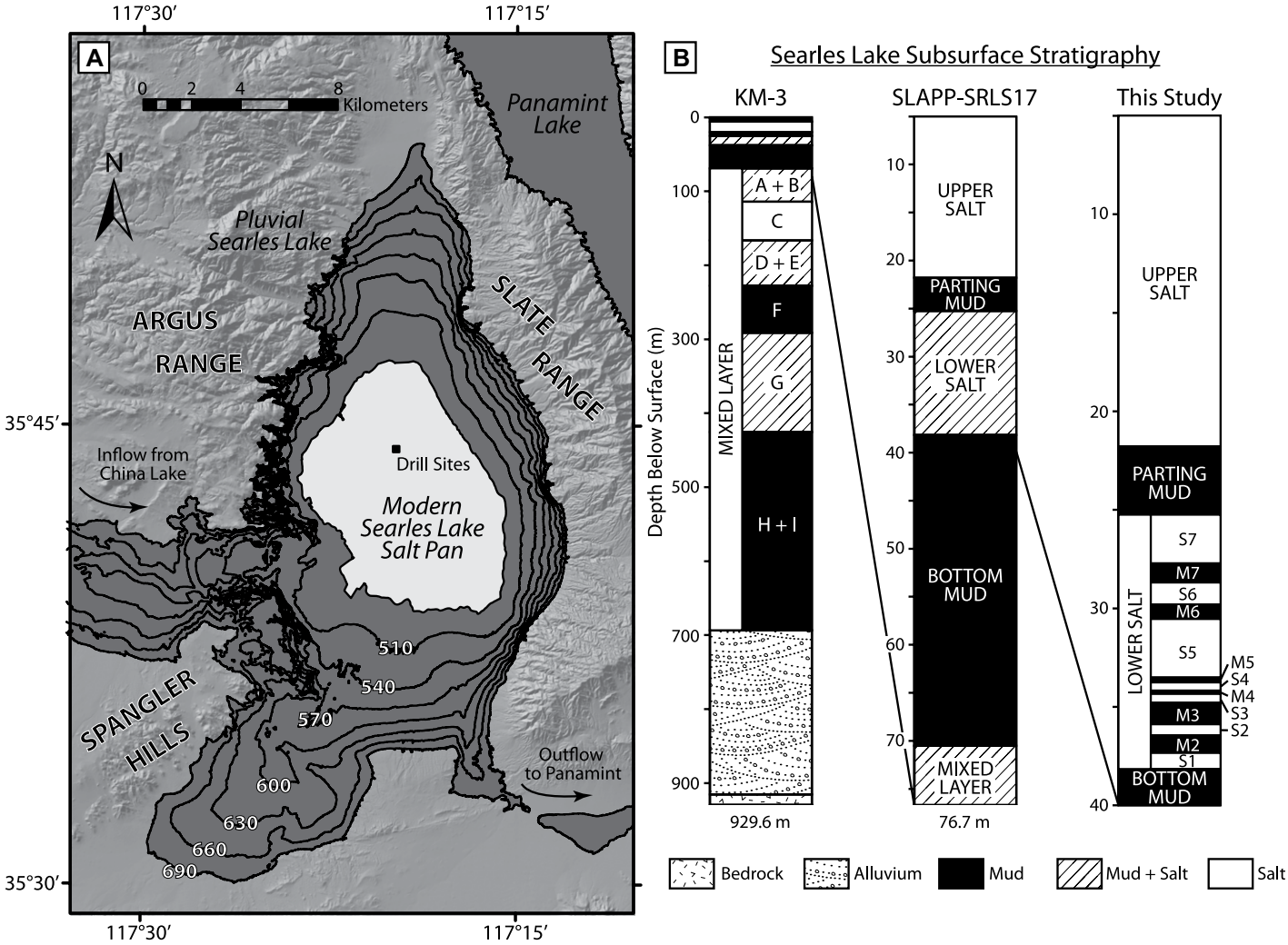

Figure 2. (A) Map of Searles Valley shows pluvial lake elevations and extent of modern salt pan and (B) Searles Lake subsurface stratigraphy from KM-3 and SLAPP-SRLS17–1A/B. Modified from Smith (1979) and Smith et al. (1983).

lake deposition (Bischoff et al., 1985). A second core, SLAPP-SRLS17-1B (−117.330298425, −117.330330804), was drilled from 21.7 mbs to 38.8 mbs to ensure complete recovery of the Lower Salt. Core description, sampling, and photography were performed in 2017 at the National Lacustrine Core Facility (LacCore) of the University of Minnesota.

Petrographic observations of core SLAPP-SRLS17 were primarily made on core photos and augmented with hand samples and thin sections. A total of 233 samples from various depths in the core were selected for X-ray diffraction (XRD) analysis with a PANalytical XPert PW3040 diffractometer operated at 40 kV and 20 mA using Cu-Kα radiation fitted with a diffracted-beam graphite monochromator. Powders were run in a continuous scan from 5.00° to 50.00° 2θ with step sizes of 0.040° at 0.80 s per step. The PANalytical software package Highscore Plus was used to identify minerals by reference peak positions and weight percentages of mineral mixtures from relative peak heights. A mineralogical profile of the 14 most common non-clastic minerals of core SLAPP-SRLS17 arranged by sample depth is shown in Figures 4A (Parting Mud and Upper Salt) and Figure 4B (Bottom Mud and Lower Salt).

EQL/EVP Model Simulations

The model code EQL/EVP was used to simulate the stepwise evaporation of Owens River

TABLE 3. LITHOSTRATIGRAPHY AND MAJOR MINERAL COMPOSITION OF THE SEARLES LAKE DEPOSIT FROM 0–38 METERS BELOW SURFACE

Unit	Depth to base* (m)	Thickness* (m)	Age of base* (ka)	Volume† (×10⁶ m³)	Major mineral mass abundance (×10¹² g)†						
					Trona	Halite	Borax	Hanksite	Gaylussite	Pirssonite	Burkeite
Overburden Mud	5.8	5.8	6	380	9	106	–	10	–	19	–
Upper Salt	19.9	14.1	10	1026	764	980	717	459	–	5	8
Parting Mud	25.0	5.1	24	480	2	–	43	–	84	33	–
Lower Salt	37.9	12.9	32	658	770	323	152	10	153	56	80

*Values for core KM-3 (Smith et al., 1983).
†Estimated from ~100 drill cores (Smith, 1979).

Downloaded from http://pubs.geoscienceworld.org/gsa/gsabulletin/article-pdf/doi/10.1130/B35857.1/5242712/b35857.pdf
by SUNY Binghamton Science Library user

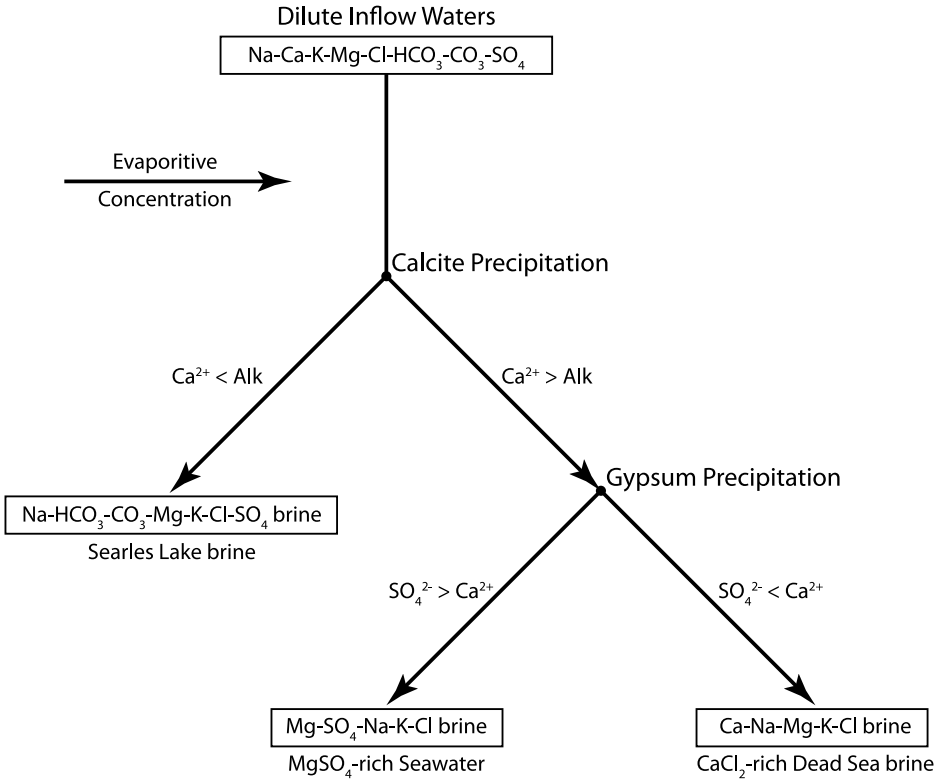

Figure 3. Principle of chemical divides diagram for dilute inflow waters is shown; adapted from Hardie and Eugster (1970).

water at a range of temperatures and pCO_2 to determine possible climatic controls on evaporite phases, sequences, and abundances. Modern Searles Valley mean daily air temperatures range from 7 °C to 32 °C (https://wrcc.dri.edu), so EQL/EVP simulations were run from 5 °C to 35 °C in 0.5–5 °C increments. Atmospheric CO_2 during Searles Lake Lower and Upper Salt deposition (32–6 ka) ranged from ~190–270 ppmv per the Vostok ice core record (Petit et al., 1999). EQL/EVP simulations were therefore run at 200 ppm pCO_2 to simulate conditions when Searles Lake was in approximate equilibrium with atmospheric CO_2. pCO_2 was then increased in 100–200 ppm increments to model periods when Searles Lake had pCO_2 concentrations greater than atmospheric values. Starting alkalinity of Owens River water was tested across the range measured by Hollett et al. (1991) (Table 2) to ascertain likely conditions of ancestral Owens River water. Additionally, EQL/EVP requires that *open* versus *closed* behavior of the system be specified. An *open* system (i.e., fractional crystallization) does not permit back-reactions between precipitates and solution, whereas a *closed* system (i.e., equilibrium crystallization) does. Each temperature/pCO_2 combination was simulated twice, once as an *open* system and once as a *closed* system, to determine the crystallization behavior for Searles Lake evaporites with and without back-reactions.

EQL/EVP begins the simulation with 55.51 mol H_2O (~1 L) of Owens River water (Table 2) at a specified temperature and pCO_2 and calculates the molality, activity, and activity coefficient of each dissolved species as well as the activity of the solvent (water). EQL/EVP performs stepwise evaporation by removing a specified percentage of water (5% used here) per step until the system becomes invariant (i.e., zero degrees of freedom). At each evaporation step, EQL/EVP calculates molalities, activity coefficients, and activities of each species and the activity of H_2O. If the solution is supersaturated with respect to a mineral, EQL/EVP determines the mass of that mineral precipitated at each evaporation step via the law of mass action. If the simulation is run as an *open* system, the precipitates are fractionally removed from the solution. Conversely, if the simulation is run as a *closed* system, the precipitates remain available through subsequent evaporation steps to back-react with the brine and form new minerals. At each evaporation step, EQL/EVP calculates the molality of each component in solution as well as the moles of each mineral precipitated.

RESULTS

Mineralogy of Core SLAPP-SRLS17

The chemical sediments of Searles Lake are classified by mineralogy and texture and can be divided into three genetic types based on the timing of their formation: (1) "early" relatively insoluble alkaline earth carbonates, (2) primary bedded evaporites, and (3) "later" diagenetic salts. The "early" alkaline earth carbonates found in core SLAPP-SRLS17 include calcite [$CaCO_3$], aragonite [$CaCO_3$], and dolomite [$CaMg(CO_3)_2$]. These minerals occur as primary laminae (Figs. 5A–5C) within the Parting Mud (Fig. 4A) and Bottom Mud (Fig. 4B) that correspond to times of relatively high lake levels (Smith, 1979, 2009).

The bedded evaporites of core SLAPP-SRLS17 occur as either (1) aggregates of fine-grained crystals that are interpreted as lake surface or water column precipitates that settled onto the lake floor as cumulates or (2) larger interlocking subhedral crystals that are interpreted as bottom-growth precipitates. Trona [$Na_2CO_3 \cdot NaHCO_3 \cdot 2H_2O$] is the most common Na-carbonate phase and occurs exclusively as fine-to-coarse acicular crystal cumulates (Figs. 5E–5F). Burkeite [$Na_6(CO_3)(SO_4)_2$] is the most common Na-sulfate and occurs as vuggy microcrystalline masses (Fig. 5F). The precise origin of burkeite is unclear due to textural ambiguity and requires further investigation. Smith et al. (1987) documented burkeite as a lake surface precipitate during the 1969–1971 flood and subsequent desiccation of Owens Lake. Crystallization of burkeite on the floor of Owens Lake was implied, but no textural descriptions were provided. Halite [NaCl] is the dominant bottom-growth evaporite and commonly occurs with interstitial cumulates of trona, burkeite, and borax [$Na_2B_4O7 \cdot 10H_2O$] (Fig. 5G). Thenardite [$NaSO_4$] is the only other mineral that displays bottom-growth textures, but it is limited to a 2 m portion of the Upper Salt (Fig. 4).

Primary bedded evaporites in the Searles Lake cores vary in mineral composition and mass abundance. However, stratigraphically, the evaporite units are interrelated through a broader depositional sequence that reflects the evolving brine composition through time. The sequence observed in the bottom half of the Lower Salt (Fig. 4B) is as follows: S1 (trona), S2 (trona, minor burkeite), S3 (trona and burkeite), and S4 (halite, minor trona/burkeite). The trona → burkeite → halite sequence is also observed at finer scales in the Upper Salt (Fig. 4A) and is therefore interpreted as the defining primary evaporite sequence for Searles Lake during the late Pleistocene/Holocene.

Downloaded from http://pubs.geoscienceworld.org/gsa/gsabulletin/article-pdf/doi/10.1130/B35857.1/5242712/b35857.pdf
by SUNY Binghamton Science Library user

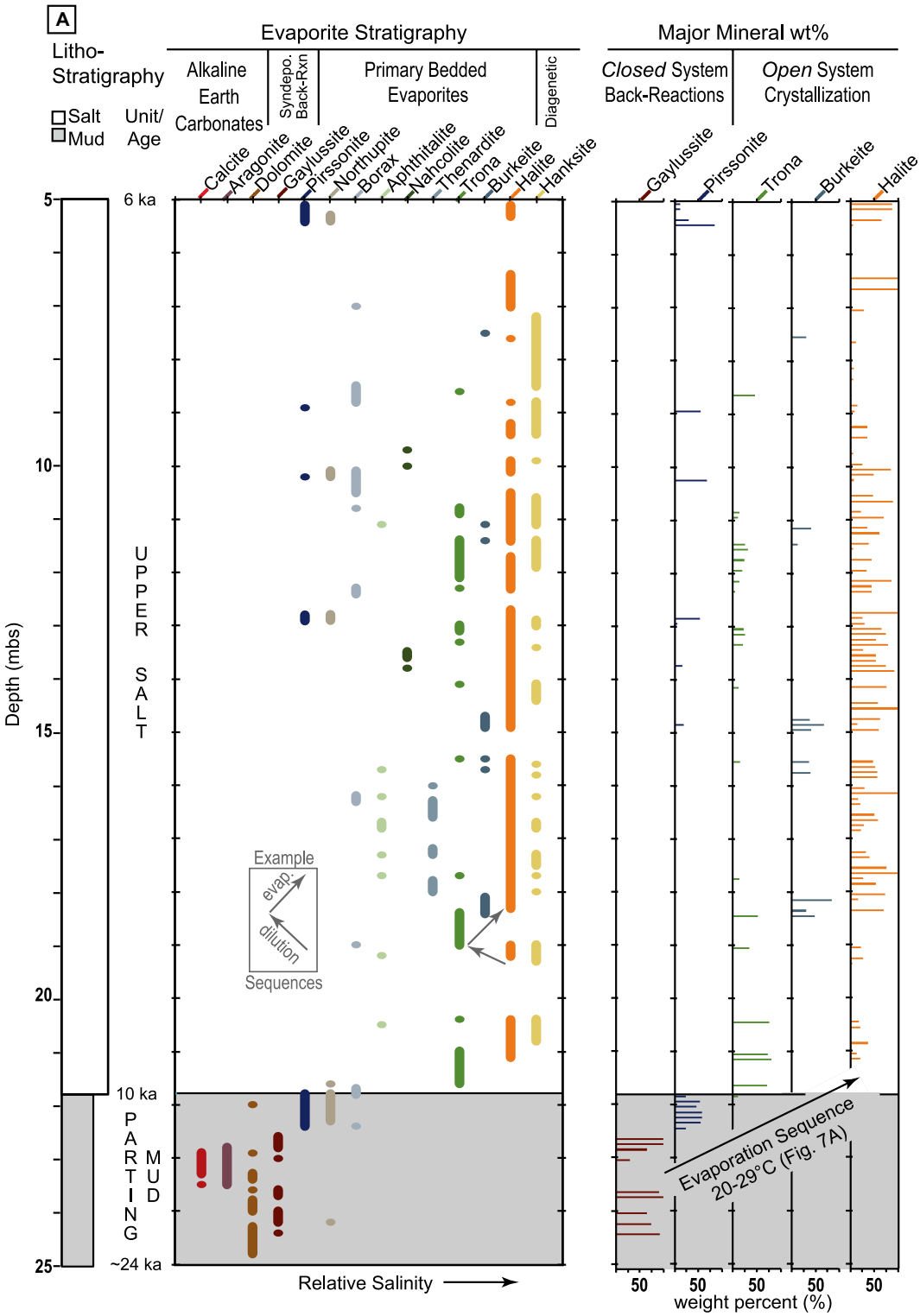

Figure 4. Stratigraphy and mineralogy of core SLAPP-SRLS17 is shown for (A) the Parting Mud and Upper Salt and (B) the Lower Salt. Lithostratigraphic units are from Smith (1979). Radiocarbon ages are from Stuiver and Smith (1979). Mineral occurrences and weight percentages are plotted for 10 cm intervals.

Intrasediment crystal growths with cross-cutting relationships and void-filling cement fabrics are interpreted as "later" diagenetic salts. These include gaylussite [$Na_2Ca(CO_3)_2 \cdot 5H_2O$], pirssonite [$Na_2Ca(CO_3)_2 \cdot 2H_2O$], and hanksite [$Na_{22}K(SO_4)_9(CO_3)_2Cl$]. Gaylussite and pirssonite occur as microscopic crystals and as megascopic sub-planar to sub-vertical euhedra that commonly cross-cut host laminations (Figs. 5B–5C) and partially to fully replace calcite/aragonite laminae (Figs. 5B–5D). Gaylussite is found throughout the Lower Salt mud units (M2–7) and the Parting Mud (Fig. 4). Pirssonite occurs in the mud units at the top of the Lower Salt (M6,7), the top of the Parting Mud, and within Upper Salt mud partings (Fig. 4). Hanksite forms randomly oriented, large (centimeter-scale) euhedral crystals within mud units and as cement within crystalline units (Fig. 5H). Hanksite first occurs at the base of the S7 unit in the Lower Salt and then is abundant in the Upper Salt (Fig. 4A).

Downloaded from http://pubs.geoscienceworld.org/gsa/gsabulletin/article-pdf/doi/10.1130/B35857.1/5242712/b35857.pdf
by SUNY Binghamton Science Library user

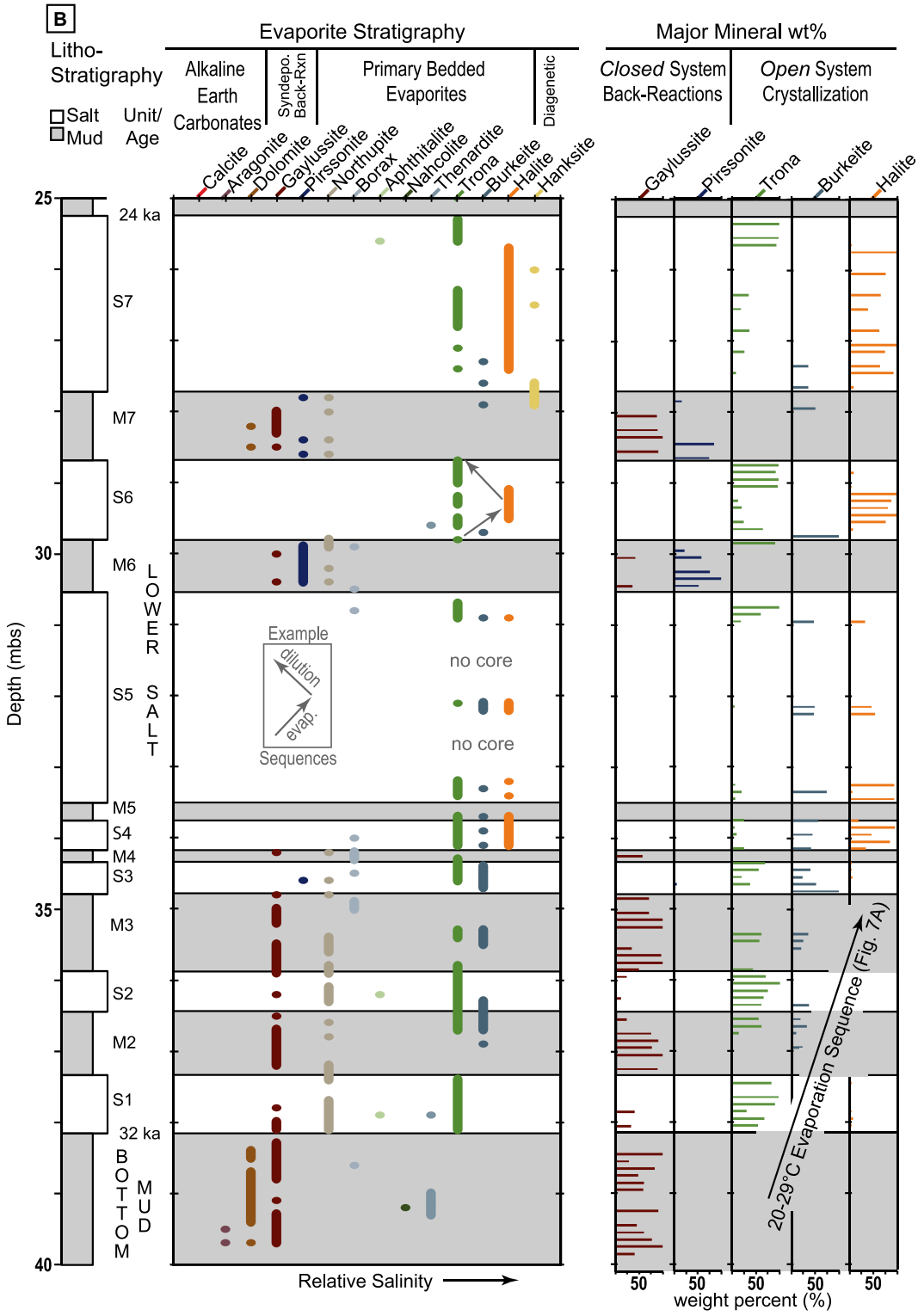

Figure 4. (Continued)

Model Results

EQL/EVP simulations of evaporating modern Owens River water produce all the major minerals observed in the Lower Salt and Upper Salt of core SLAPP-SRLS17 but require crystallization to occur in both *open* and *closed* systems. Simulated brine evolution and mineral precipitation is therefore divided into three parts based on the order and process of mineral formation (Fig. 6). The first stage of simulated brine development is the precipitation of early insoluble alkaline earth carbonates, which occurs regardless of *open* or *closed* system behavior (Fig. 6A). Simulations then proceed with either (2) *open* system fractional crystallization (Fig. 6B) or (3) *closed* system back-reactions (Fig. 6C).

Downloaded from http://pubs.geoscienceworld.org/gsa/gsabulletin/article-pdf/doi/10.1130/B35857.1/5242712/b35857.pdf
by SUNY Binghamton Science Library user

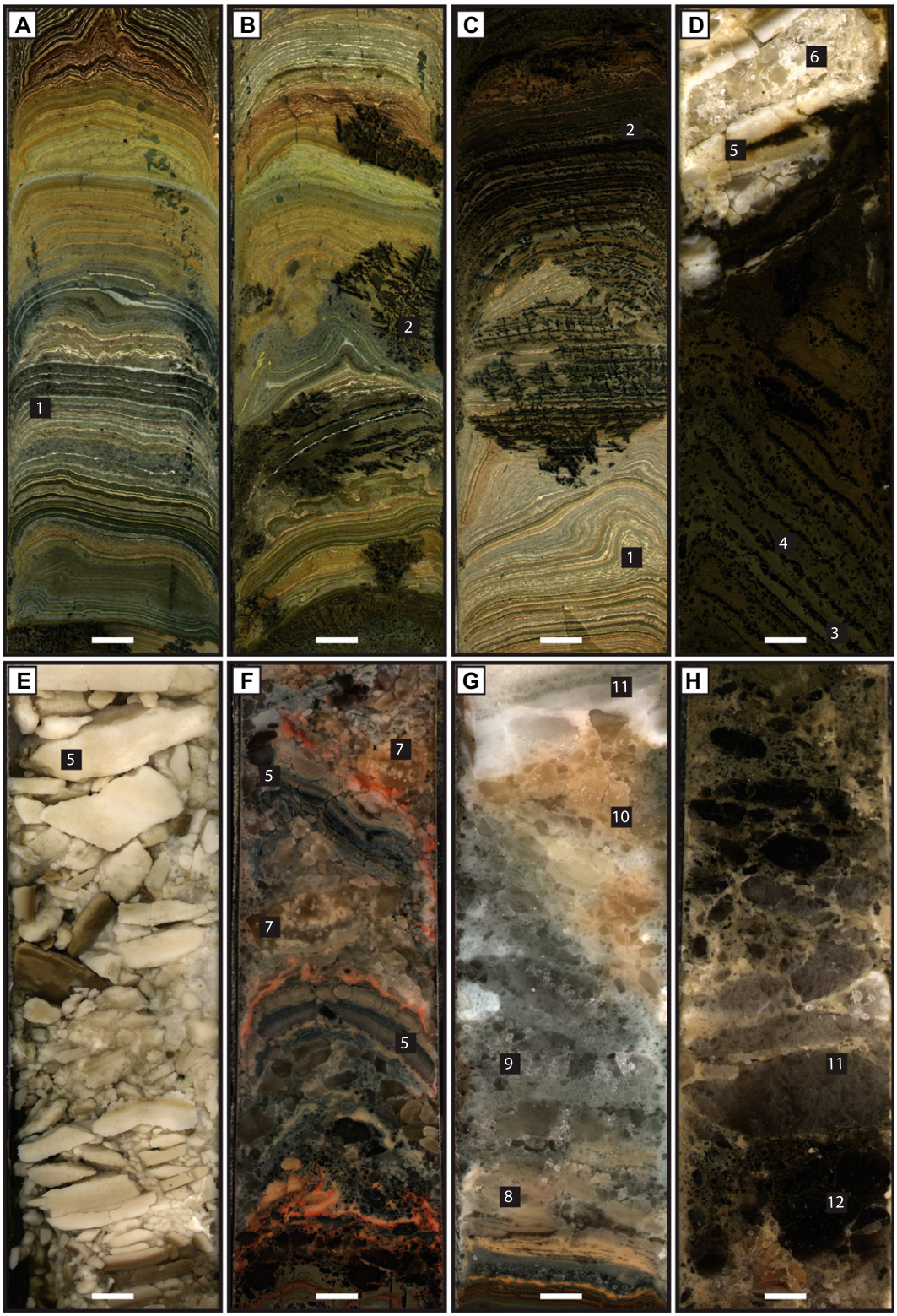

Figure 5. Photographs show core SLAPP-SRLS17 post-oxidation. Each image represents 30 cm × 10 cm (scale bar = 2 cm). All fractured and non-horizontal layering is assumed to be an artifact of vibracoring. (A) Laminated alkaline earth carbonates [1] and detrital muds [Parting Mud; 23.32–23.62 mbs]. (B) Duplicate core overlapping with (A) (~3 m horizontal offset) shows partial replacement of alkaline earth carbonates with macroscopic gaylussite [2] [Parting Mud; 23.29–23.59 mbs]. (C) Transition of unaltered alkaline earth carbonates [1] to full replacement of $CaCO_3$ by gaylussite [2] [Parting Mud; 22.17–22.47mbs]. (D) Dark laminae of macrocrystalline pirssonite [3] interlayered with microcrystalline northupite in green mud [4], transitioning to layered trona [5] and borax [6] [Parting Mud/Upper Salt; 21.47–21.77 mbs]. (E) Bedded cumulate trona [5] [Upper Salt; 21.29–21.59 mbs]. (F) Interbedded cumulate trona [5] and vuggy burkeite [7]. Pink muds indicate carotenoids [Lower Salt (S3); 34.4–34.7 mbs]. (G) Mixed trona + burkeite + halite [8] → halite and borax [9] → halite + burkeite [10] → halite [11] [Lower Salt (S4); 33.78–34.08 mbs]. (H) Bottom-growth halite [11] interlayered with hanksite [12] [Upper Salt; 12.52–12.82 mbs].

EQL/EVP model simulations were performed at constant temperature and pCO_2, using high values of alkalinity (2.8 mmol/kg H_2O) to reproduce the observed carbonate and sulfate-bearing mineral sequences. Figure 6 shows example simulations run at 23 °C with pCO_2 set to 200 ppm; evaporation progresses from left to right (i.e., decreasing aH_2O). The effect of temperature and pCO_2 on the type and order of minerals formed can be assessed by compiling phase diagrams from multiple EQL/EVP simulations. Figure 7 shows phase diagrams classified by pCO_2 and system behavior (*open* versus *closed*) with temperature and aH_2O as the independent variables. Individual simulations are represented in the

Downloaded from http://pubs.geoscienceworld.org/gsa/gsabulletin/article-pdf/doi/10.1130/B35857.1/5242712/b35857.pdf
by SUNY Binghamton Science Library user

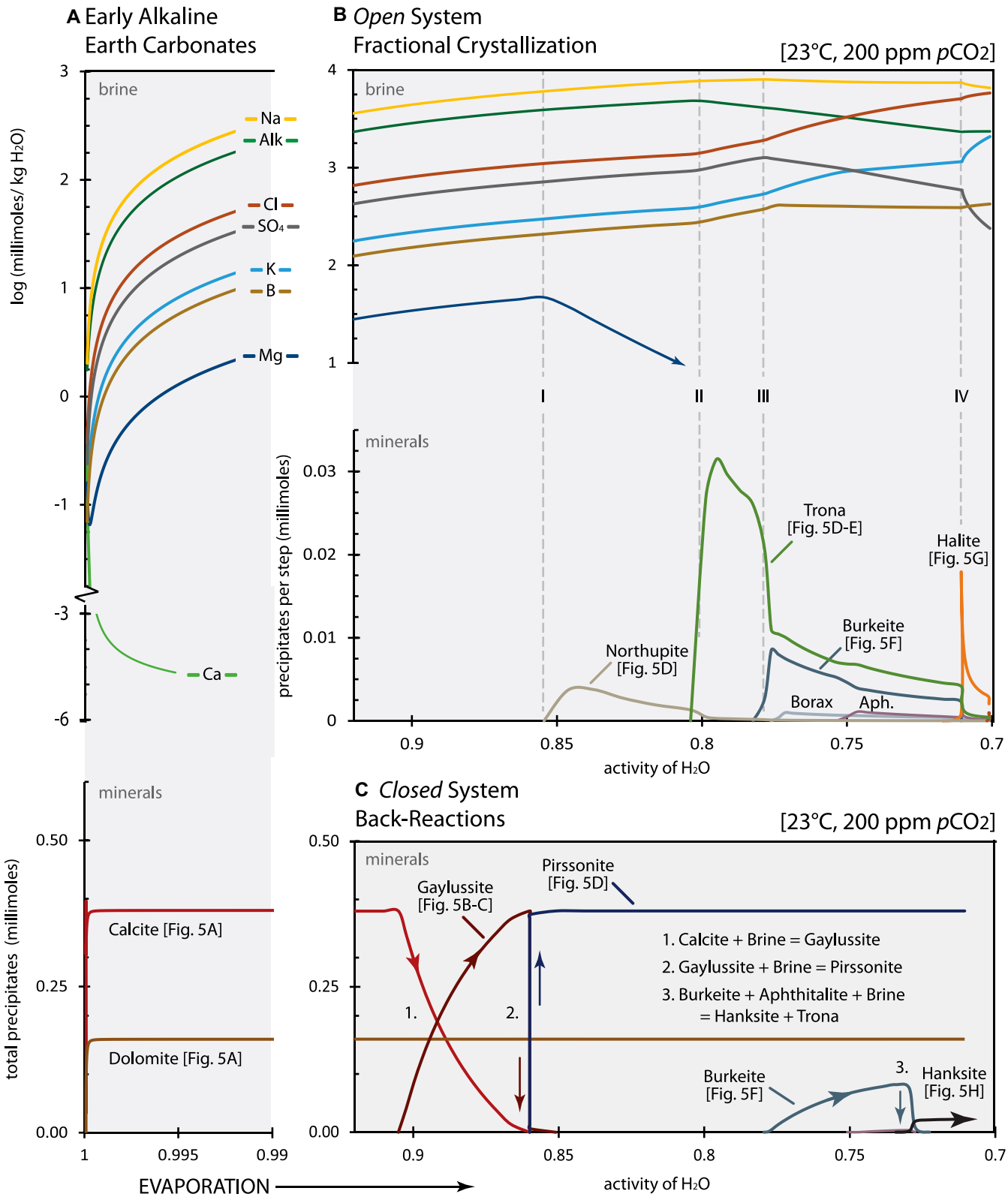

Figure 6. Example of equilibrium program/evaporation program (EQL/EVP) simulations is shown for evaporating Owens River water at 23 °C and 200 ppm pCO_2. X axes of (B) and (C) are equally scaled and aligned. (A) Initial brine development as early alkaline earth carbonates are fractionally removed, and evaporation begins. (B) Brine chemistry (top) and mineral precipitation (bottom) during *open* system fractional crystallization. Aph.—aphthitalite. (C) *Closed* system back-reactions of [1] $CaCO_3$ → gaylussite, [2] gaylussite → pirssonite, and [3] burkeite + aphthitalite → hanksite. Note: trona and halite near reaction 3 are removed for figure clarity; aphthitalite is plotted but minor in scale.

Downloaded from http://pubs.geoscienceworld.org/gsa/gsabulletin/article-pdf/doi/10.1130/B35857.1/5242712/b35857.pdf
by SUNY Binghamton Science Library user

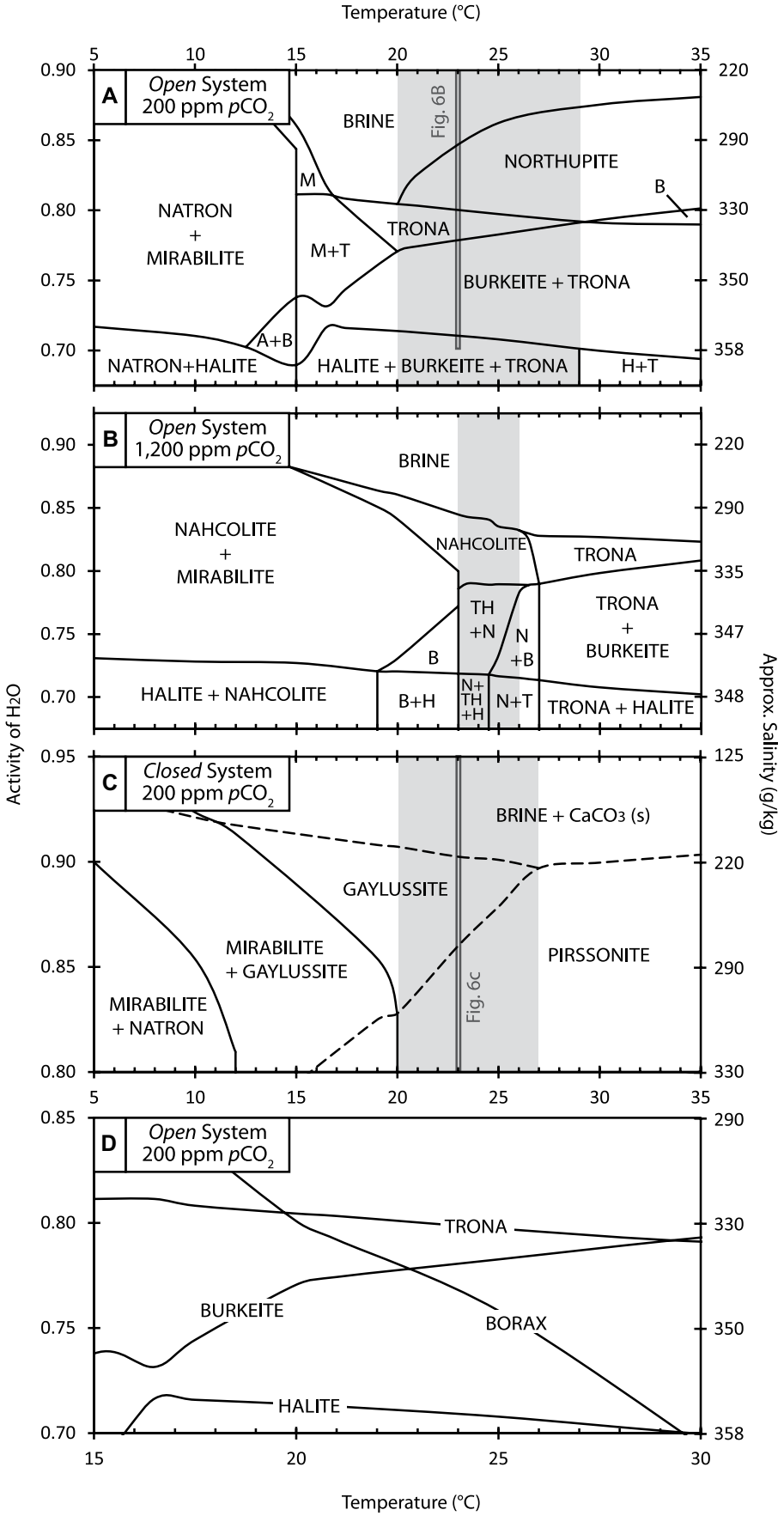

Figure 7. Phase diagrams show the evaporation of Owens River water. (A) *Open* system, fractional crystallization at 200 ppm pCO_2. (B) *Open* system, fractional crystallization at 1200 ppm pCO_2. (C) *Closed* system back-reactions at 200 ppm pCO_2; black dashed lines indicate crystal/brine reaction boundaries. (D) Onset of borax precipitation compared to trona, burkeite, and halite at 200 ppm pCO_2. Gray shading corresponds to mineral sequences observed in core SLAPP-SRLS17. Salinities are shown for 23 °C. A—natron, B—burkeite, H—halite, M—mirabilite, N—nahcolite, T—trona, TH—thenardite.

phase diagrams by single vertical slices (i.e., isotherms); evaporation proceeds down the *y*-axis toward higher salinity and lower aH_2O. For example, the simulations in Figure 6 are highlighted as gray, double lines in Figure 7. Phase boundaries indicate the onset or termination of mineral precipitation, and each field indicates which phase(s) precipitate.

Early Alkaline Earth Carbonates: The Pre-Evaporite Sequence

Modern Owens River water, like many dilute natural waters, is supersaturated with respect to calcite, aragonite, and dolomite at 23 °C. The first stage of EQL/EVP simulations involves iterations to equilibrate Owens River water by precipitating supersaturated phases until equilibrium conditions are established. Virtually all $CaCO_3$, as calcite or aragonite, is precipitated during the initial equilibration and prior to any evaporation. If dolomite precipitation is enabled during EQL/EVP simulations, then dolomite precipitates alongside $CaCO_3$ during the initial equilibration. Consequently, when the evaporation program begins and ionic concentrations are increased, Ca^{2+} and Mg^{2+} are already significantly depleted, and the bulk of the calcite (0.38 mmoles) and dolomite (0.16 mmoles) is already precipitated (Fig. 6A).

Open System Crystallization: The Layered Evaporites

Following the initial removal of alkaline earth carbonates, evaporating Owens River water will increase in ionic concentration until soluble salts reach saturation at ≤ 0.9 aH_2O (Figs. 6A–6B). If sufficient Mg^{2+} remains in solution, northupite [$Na_3Mg(CO_3)_2Cl$] precipitates as the first *open* system salt at ~0.85 aH_2O (Figs. 6B and 5A). If dolomite precipitation is inhibited kinetically (see Peterson and Bien, 1966), then northupite becomes the default Mg-bearing salt and precipitates in

Downloaded from http://pubs.geoscienceworld.org/gsa/gsabulletin/article-pdf/doi/10.1130/B35857.1/5242712/b35857.pdf
by SUNY Binghamton Science Library user

large amounts beginning at ~0.9 aH_2O salinity at all temperatures and CO_2 concentrations. In either case, Mg^{2+} is fractionally removed from the brine during northupite precipitation until the evaporating brine becomes saturated with Na-carbonate (e.g., trona) and Na-sulfate (e.g., burkeite) (Fig. 6B). However, the specific Na-carbonate and Na-sulfate minerals formed (trona versus nahcolite [$NaHCO_3$]; burkeite versus thenardite), and their order of precipitation, are controlled by the temperature and pCO_2 of the evaporating brine.

Figures 5A and 5B show the *open* system minerals and sequences as a function of temperature and aH_2O for 200 ppm and 1200 ppm pCO_2, respectively. At 200 ppm pCO_2, simulating Searles Lake brine in equilibrium with late Pleistocene atmospheric CO_2, Na-carbonate precipitation precedes Na-sulfate precipitation between 16 °C and 29 °C. The sequence northupite → trona → burkeite → halite further constrains precipitation temperatures to 20–29 °C (Fig. 7A, shaded). At 1200 ppm pCO_2, approximately six times late Pleistocene atmospheric values, the Na-carbonate → Na-sulfate sequence persists, but nahcolite forms instead of trona (at temperatures below 27 °C), and thenardite is the Na-sulfate phase at temperatures of 23–26 °C. Evaporation at 23 °C, for example, produces nahcolite → thenardite → halite (Fig. 7B, shaded). EQL/EVP models for evaporating Owens River water therefore demonstrate that the Na-carbonate → Na-sulfate sequence constrains temperature while the Na-carbonate phase (trona versus nahcolite) and Na-sulfate phase (burkeite versus thenardite) constrain the pCO_2.

Minor *open* system minerals include borax and aphthitalite [$K_3Na(SO_4)_2$]. As non-carbonates, and the sole B- and K-bearing phases, these minerals behave more or less independently of brine evaporation dynamics and pCO_2. Borax precipitation is strongly temperature dependent (Fig. 7D) and forms prior to Na-carbonates at temperatures below 20 °C, with trona/burkeite at temperatures ≥23 °C, and alongside halite at 30 °C. Borax as an associated mineral is therefore useful as a general temperature indicator. Aphthitalite typically forms after mirabilite/burkeite and is important as a precursor to hanksite diagenesis (see below).

Closed System Back-Reactions: The Chemical Overprints

A *closed* system maintains contact with, and equilibrium between, the evaporating aqueous solution and previously precipitated minerals, therefore allowing salinity-driven back-reactions. During the *closed* system evaporation of Owens River water, the early-formed calcite/aragonite (but not dolomite) back-react with the subsequently concentrated Na-rich brine to form gaylussite [$Na_2Ca(CO_3)_2 \cdot 5H_2O$] (Figs. 6C and 5C). As evaporation continues and aH_2O decreases, an additional back-reaction occurs whereby gaylussite partially dehydrates to pirssonite [$Na_2Ca(CO_3)_2 \cdot 2H_2O$] (Fig. 6C and 5C). Above 27 °C, pirssonite forms directly from the calcium carbonate phase (Fig. 7C).

Additional *closed* system back-reactions occur at higher salinities involving the formation of hanksite [$Na_{22}K(SO_4)_9(CO_3)_2Cl$] (Fig. 6C). Hanksite forms from ~18–24 °C at 200 ppm pCO_2 and ~20–30 °C at 1200 ppm pCO_2. The formation of hanksite varies based on brine chemistry and available precipitates for back-reaction. If available, hanksite consumes aphthitalite as a source of K^+ rather than obtaining K^+ from the brine. Hanksite completely consumes burkeite/thenardite as the primary source of SO_4^{2-} (i.e., the limiting factor for hanksite precipitation).

DISCUSSION

Searles Lake Evaporite Sequence

The requirement of both *open* and *closed* system behavior to account for all SLAPP-SRLS17 phases highlights the different mechanisms of chemical sedimentation in Searles Lake. *Open* and *closed* system behavior closely follow the well-known lithostratigraphy of Smith (1979), where *open* system crystallization produces the "crystalline" salt units and *closed* system back-reactions produce the abundant gaylussite and pirssonite found in mud units (Fig. 4). *Open* systems, therefore, are characterized by precipitation from the water column, whereas *closed* systems are characterized by in situ back-reactions between *open* system precipitates and interstitial brine.

Open system, fractional crystallization of Owens River water produces all the primary chemical sediments found in Searles Lake. Alkaline earth carbonates (calcite, aragonite, dolomite) precipitate from the water column as relatively freshwater phases and form laminated chemical muds on the lake floor (Fig. 5A). $CaCO_3$ and $CaMg(CO_3)_2$ precipitation fractionally removes Ca^{2+} and Mg^{2+} from solution, so Searles Lake brine evolves toward a Na-CO_3-K-B-Cl-SO_4^{2-} composition (Fig. 6A). Residual Mg^{2+} is fractionally removed by northupite precipitation while remaining components increase in concentration (Fig. 6B: I→II). As Mg^{2+} is depleted, the brine reaches saturation with respect to trona and begins fractionally removing Na^+, HCO_3^-, and CO_3^{2-} (Fig. 6B: II→III), followed by precipitation of burkeite, which fractionally removes Na^+ and SO_4^{2-} (Fig. 6B: III→IV). K^+ and BO_3^{3-} are depleted by the precipitation of aphthitalite and borax, respectively. Halite saturation is reached when CO_3^{2-} and SO_4^{2-} are depleted and Cl^- becomes the dominant anion (Fig. 6B: IV).

The prevalence of gaylussite/pirssonite in the mud units and hanksite cement in the crystalline units (Fig. 4) indicates that *closed* system back-reactions must also occur, although the timing and mechanisms of the back-reactions differ. $CaCO_3$ back-reactions occur when freshwater carbonates are deposited as laminated muds and subsequent saline lake waters permeate through underlying sediment and react to form gaylussite or pirssonite (Figs. 5A–5D). The solute flux required for in situ back-reactions is likely driven by a density gradient, as observed in Great Salt Lake cores (Spencer et al., 1985), in which more saline, higher density brine sinks and diffuses through less saline, lower density pore fluids. The salinity required for $CaCO_3$ back-reactions is slightly below that required for northupite precipitation; thus, gaylussite back-reactions occur contemporaneously with, or as a precursor to, northupite precipitation (Figs. 6B–6C). If density-driven solute fluxes occurred without constraint as lake brines evolved through northupite to trona + burkeite + halite saturation, then all gaylussite would be replaced by pirssonite (Figs. 5C and 6C). The occurrence of gaylussite in most mud units, and the preservation of $CaCO_3$ in the Parting Mud and Bottom Mud (Fig. 4), however, suggest a limit on density diffusion, likely due to decreasing permeability in response to early compaction. Thus, gaylussite formed during $CaCO_3$ back-reactions must occur early, prior to mud compaction, and is therefore interpreted as syndepositional. The syndepositional origin of gayussite and pirssonite is important, as it suggests the minerals reflect lake water temperatures and salinities and preserves this record in approximate stratigraphic order. Early back-reaction minerals therefore fall within the primary evaporite sequence as calcite/aragonite (Fig. 6A) → gaylussite (Fig. 6C) → northupite/pirssonite (Figs. 6B–6C), as observed in the Parting Mud and Bottom Mud (Fig. 4).

The precise timing of hanksite cementation is less clear. Model simulations predict that hanksite forms by back-reaction prior to halite saturation. Texturally, however, hanksite generally occurs as a post-halite, void-filling cement. This may be due to the slow kinetics of hanksite crystal growth (Teeple, 1929). The lack of compaction in hanksite-cemented units suggests early, pre-compaction diagenesis. It is possible that hanksite precipitation was slow and began syndepositionally, as predicted by the model, and continued as a cement in the Searles evaporite sequence. The complete Searles Lake

Downloaded from http://pubs.geoscienceworld.org/gsa/gsabulletin/article-pdf/doi/10.1130/B35857.1/5242712/b35857.pdf
by SUNY Binghamton Science Library user

mineral sequence with respect to timing of mineral precipitation, and including back-reactions, is as follows: alkaline earth carbonates (Fig. 6A) → gaylussite (Fig. 6C) → northupite/pirssonite (Figs. 6B–6C) → trona/burkeite/halite (Fig. 6B) → hanksite diagenesis (Fig. 6C).

Indicators of pCO_2

Na-carbonate evaporites have been established as reliable proxies for lake water pCO_2 that can be used to reconstruct atmospheric paleo-CO_2 records by assuming equilibrium between the atmosphere and lake water (e.g., Jagniecki et al., 2015). However, the concentration and behavior of CO_2 in lakes—and especially in saline-alkaline lakes—is poorly understood. The calculated surface water pCO_2 from a global survey of modern saline lakes showed that water body pCO_2 exceeded modern atmospheric values by five to eight times on average, which led to the conclusion that saline lakes in general are net emitters of CO_2 (Duarte et al., 2008). However, the pCO_2 of Owens Lake during the 1969–1971 flood started at six times atmospheric pressure at lake high stand and ended at 0.02 times atmospheric pressure during the final stages of desiccation (Smith et al., 1987). Saline-alkaline lakes can thus emit or absorb CO_2. Here, the record of Searles Lake pCO_2 derived from evaporite proxies is compared with the contemporaneous record of atmospheric CO_2 derived from ice cores to assess the state of equilibrium between the two.

Atmosphere CO_2 concentration during the past 32–6 ka was ~190–270 ppmv (Petit et al., 1999). If Searles Lake contained five to eight times atmospheric pCO_2 (per Duarte et al., 2008), then the Na-carbonates and Na-sulfates of core SLAPP-SRLS17 would be predominantly nahcolite and thenardite (Fig. 7B). While these phases exist in the core, they are nonetheless rare, appearing only in a thin layer of the Bottom Mud (Fig. 4B) and three layers in the Upper Salt (Fig. 4A), totaling only ~3.5 m of the upper 40 m of SLAPP-SRLS17. Instead, the dominant Na-carbonate and Na-sulfate phases in the SLAPP-SRLS17 core are trona and burkeite, respectively, which are stable at the lower range of pCO_2 conditions and consistent with contemporaneous atmospheric values (Fig. 7A).

Rare episodes of lake water pCO_2 exceeding three times atmospheric CO_2 (>700–800 ppm) are indicated by layers of nahcolite and thenardite (Fig. 4A). High concentrations of CO_2 in lakes can be attributed to biologic respiration, carbonate precipitation, and hydration of atmospheric CO_2 by hydroxide ions in the alkaline surface water (Cole et al., 1994; Barkan et al., 2001; Wanninkhof and Knox, 1996). These processes were probably important controls of the lake water pCO_2 at Searles Lake. The sparse and irregular high-pCO_2 spikes may also be explained by variable outgassing of CO_2 directly into Searles Lake bottom waters along faults. Fault-controlled CO_2 outgassing has been measured at 1056 ± 581 ppm in the Magadi Basin of Kenya (Lee et al., 2016) and is considered the best explanation for nahcolite-saturation in East African Rift lakes, such as Nasikie Engida, Kenya (De Cort et al., 2019; Renaut et al., 2020). We speculate that outgassing at Searles Lake along faults may be recorded by the sharp, lateral shifts between trona and nahcolite parallel to the Argus Mountains (Fig. 1) (Jade Brush, personal correspondence, 2018). Trona and nahcolite within the same horizontal unit indicates two pCO_2 regimes existing simultaneously within the lake. The sharp lateral transition of the phases suggests, and is best explained by, fault-control. Although no measurements of CO_2 fluxes have been made in the Searles Basin, earthquakes in 2019 indicate active faulting (Ross et al., 2019). The Searles Lake record further establishes the usefulness of evaporites as proxies for pCO_2 as well as the need to better understand the role of CO_2 in saline-alkaline lake systems.

Indicators of Paleotemperature

Phase diagrams showing the evaporation of Owens River water (Fig. 7) demonstrate the sensitivity of evaporite precipitation to brine temperature, which supports the applicability of the Searles Lake mineralogical record as a proxy for paleobrine temperatures.

At 200 ppm pCO_2, an Na-carbonate phase boundary occurs at 15 °C, above which trona precipitates and below which natron [$Na_2CO_3 \cdot 10H_2O$] forms (Fig. 7A). The predominance of trona and absence of natron in the SLAPP-SRLS17 core indicates paleobrine temperatures >15 °C. Similarly, the Na-sulfate salt burkeite in the SLAPP-SRLS17 core and the lack of mirabilite [$Na_2SO_4 \cdot 10H_2O$] indicate paleobrine temperatures >20 °C (Fig. 7A). A 20 °C minimum temperature is also indicated by northupite (Fig. 7A). Paleobrine temperatures can be further constrained by the relative order of Na-carbonate and Na-sulfate precipitation. In core SLAPP-SRLS17, trona precedes burkeite in the Lower Salt and Upper Salt: trona → burkeite → halite (Fig. 4), which indicates brine temperature between 20 °C and 29 °C (Fig. 7A, shading). Less alkaline parent Owens River water (e.g., 2.8 mmol/kg H_2O) narrows this brine temperature range by several degrees. Similarly, if dolomite precipitation is inhibited, then burkeite saturation is reached at slightly lower salinities and the trona → burkeite → halite sequence is narrowed to 20–26 °C. Borax can further constrain brine temperatures. Where borax formed before trona, brine temperatures must be ≤20 °C (Fig. 7D) (e.g., Bottom Mud and Parting Mud/Upper Salt transition). Alternatively, borax associated with halite (e.g., the Upper Salt) suggests brine temperatures approaching, but not exceeding, 30 °C. During periods of elevated pCO_2, temperature estimates are further constrained by the 2 m of thenardite in the Upper Salt (Fig. 4A), which, according to the models, precipitates between ~23 °C and 26 °C (Fig. 7B, shading).

If *closed* system back-reactions are syndepositional, then the temperature of the back-reaction reflects lake bottom-water temperatures. If pirssonite in the Lower Salt, Parting Mud, and Upper Salt formed directly from $CaCO_3$, then lake water temperatures were above 27 °C (Fig. 7C). Alternatively, pirssonite can form at lower temperatures by salinity-driven dehydration of gaylussite (Figs. 6C and 5C, shaded). In the Parting Mud, pirssonite occurs just below the contact with the Upper Salt (Fig. 4A), where high-salinity lake water would be expected to flux through underlying sediment and produce pirssonite via dehydration of gaylussite. Likewise, pirssonite in the Upper Salt and uppermost Lower Salt coincides with periods when Searles Lake was hypersaline, again suggesting that pirssonite correlates to higher salinities (i.e., back-reactions from gaylussite) rather than higher temperatures. Additionally, pirssonite is found in conjunction with borax (Fig. 4), which supports low temperature formation of pirssonite. The *closed* system, syndepositional minerals from Searles Lake therefore formed at temperatures that are consistent with those indicated by the *open* system bedded evaporites.

Based on these interpretations of the mineral suite in the SLAPP-SRLS17 core for the 32–6 ka period, the temperature of Searles Lake waters likely varied only within a narrow ~6–9 °C range. Such a narrow temperature range implies a deep-water body sufficient to maintain thermal insulation. The control of lake depth on bottom-water temperature can be determined from modern saline lakes. Deep lakes maintain constant bottom-water temperatures. For example, the ~300-m-deep modern Dead Sea maintains a constant 24 °C bottom-water temperature (Sirota et al., 2017), which is close to the Dead Sea mean annual air temperature (Hecht and Gertman, 2003; Hamdani et al., 2018). In contrast, shallow lakes display variable bottom water temperatures that reflect seasonal air temperatures. An example of the behavior of shallow lakes with respect to seasonal air temperatures was observed in the 2.4-m-deep water body that formed following the flood of Owens Lake in 1969, where bottom water temperatures ranged

Downloaded from http://pubs.geoscienceworld.org/gsa/gsabulletin/article-pdf/doi/10.1130/B35857.1/5242712/b35857.pdf
by SUNY Binghamton Science Library user

from ~5–27 °C (Friedman et al., 1976) and mean monthly air temperatures ranged from 2 °C to 28 °C (Smith et al., 1987). If Searles Lake was shallow and bottom waters experienced the range of mean daily air temperatures of modern Searles Valley (7–32 °C), then the mineralogical record would show (1) abundant mirabilite and natron, (2) Na-sulfate minerals regularly preceding Na-carbonates, and (3) periodic alternations between pirssonite and gaylussite. Instead, the phases and sequences in core SLAPP-SRLS17 indicate long-term temperature stability of Searles Lake bottom waters that is characteristic of saline lakes with depths >10 m (e.g., Wurtsbaugh and Berry, 1990).

Lastly, the absence of natron and mirabilite may be due to temperature-driven diagenesis whereby wintertime cumulates of natron and mirabilite change to trona and burkeite, respectively, to equilibrate to stable bottom-water temperatures. However, such changes must still record observed Na-carbonate → Na-sulfate sequences and therefore only extend the lower temperature range to ~16.5 °C (Fig. 7A). A higher frequency temperature record for Searles Lake could therefore be constructed by combining additional temperature proxies with a model for temperature-driven diagenesis of evaporite minerals.

Brine Evolution and Hydrologic Implications

Searles Lake evaporites record paleohydrologic variability, where alternating units of salt and mud mark inflections in the rates of precipitation (rainfall) versus evaporation (P/E) (i.e., P > E = mud; P < E = salt). Hypothetically, if each mud-salt pair represented the flooding and subsequent desiccation of Searles Lake, then inflow volume and P/E could be calculated from the depositional ages and salt masses. However, sedimentological analysis of core SLAPP-SRLS17 has failed to yield evidence of lake desiccation, indicating that a perennial lake persisted through multiple episodes of evaporative drawdown. The significance of long-term perennial lake status is that (1) each salt unit represents only *partial* evaporation of Searles Lake and (2) younger salt beds are genetically related to older salt beds via long-term brine evolution.

An example of incomplete evaporation is seen in trona-dominated bed S1 (Fig. 4B), which records a time when Searles Lake evaporated to trona supersaturation but not beyond. Following trona precipitation, Searles Lake was diluted, and the M2 mud unit was deposited. Brine dilution is also observed in core SLAPP-SRLS17 as "reverse" evaporite sequences. For instance, the bottom half of S6 (Fig. 4B) shows the evaporite sequence trona → burkeite → halite, but the sequence reverses with trona capping the unit, which indicates a decrease in salinity. Thus, vertical transitions from evaporation sequences to dilution sequences in core SLAPP-SRLS17 indicate that P/E inflection points occurred *within* salt units and not at salt/mud contacts. Dilution sequences are important hydrologic indicators especially in the Upper Salt, where mud partings are sparse (Fig. 4A) and repeated episodes of incomplete evaporation and dilution have important effects on the long-term evolution of Searles Lake brine.

Mineral precipitation causes the relative ionic composition of evolving Searles Lake brine to diverge from the initial Owens River chemistry. For example, Owens River water contains on average 1.99 mmol/kg H_2O alkalinity and 0.37 mmol/kg H_2O Cl^-, which gives it an Alk/Cl^- of 5.4 (Table 2). But trona precipitation and loss of HCO_3^- and CO_3^{2-} eventually leads to equality of alkalinity and chlorinity (~3200 mmol/kg H_2O, Alk/Cl^- = 1) at aH_2O ≈0.75 (Fig. 6B). At that point, Owens River water had been concentrated ~9000 times by evaporation. Figure 8 shows the effect of adding dilute Owens River water to concentrated Searles Lake brine (aH_2O = 0.75 in Fig. 6B). Because the ionic concentration is so high in Searles Lake relative to the Owens River, a one-to-one mixture of Owens River water and the above 0.75 aH_2O Searles brine will produce a brine with Alk and Cl^- equal to ~1625 mmol/kg H_2O. The Alk to Cl^- ratio remains ~1 because of the huge difference in ionic strength between Owens River water and Searles Lake brine. 1000 kg of Owens River water added to 1 kg of Searles brine will produce a solution with 5.4 mmol/kg H_2O Alk and 3.5 mmol/kg H_2O Cl^-, which is significantly diluted compared to the original brine, but the Alk/Cl^- still only rises to ~1.5. Figure 8 shows the huge volume of Owens River water (~10^5 kg) that is required to dilute 1 kg of concentrated Searles brine and produce a mixture with the same ionic ratios as Owens River water. Therefore, while Searles Lake may have been diluted between times of evaporite deposition, the relative ionic composition of the lake water was not necessarily reset to initial Owens River conditions. The resultant evaporite mineral sequence formed from evaporation of these diluted brines reflects the chemistry of the hybrid Searles Lake brine/Owens River mixture and not "pristine" Owens River water.

Evaporation and mineral precipitation cause the relative ionic composition of evolving Searles Lake brines to diverge from the initial Owens River chemistry. For example, Owens River alkalinity is more than five times the chloride concentration (Table 2), but in Figure 6B, due to trona precipitation and loss of HCO_3^- and CO_3^{2-}, the alkalinity and chlorinity become equal at aH_2O ≈0.75. If this evaporation sequence is now interrupted by the addition of Owens River water, then the chemistry of the diluted brine is determined by the degree of initial evaporation, and the relative masses of lake brine and Owens River inflow. Figure 8 shows the effect of adding Owens River water to a trona-saturated lake (aH_2O = 0.75 in Fig. 6B); ~10^5 units of Owens River water are required to dilute one unit of concentrated brine and

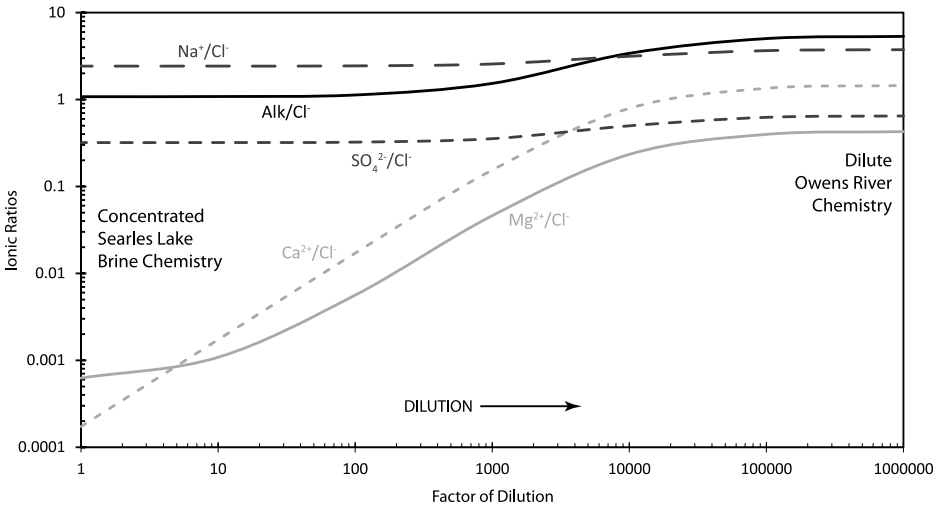

Figure 8. Diagram shows dilution of concentrated Searles Lake brine with fresh Owens River water. Factor of dilution = X kg of Owens River water (Table 2) to 1 kg Searles Lake brine. Searles Lake brine chemistry is selected where Alk/Cl^- = 1 when simulated at 23 °C, 200 ppm pCO_2 to aH_2O ≈0.75 (see Fig. 6B).

Downloaded from http://pubs.geoscienceworld.org/gsa/gsabulletin/article-pdf/doi/10.1130/B35857.1/5242712/b35857.pdf
by SUNY Binghamton Science Library user

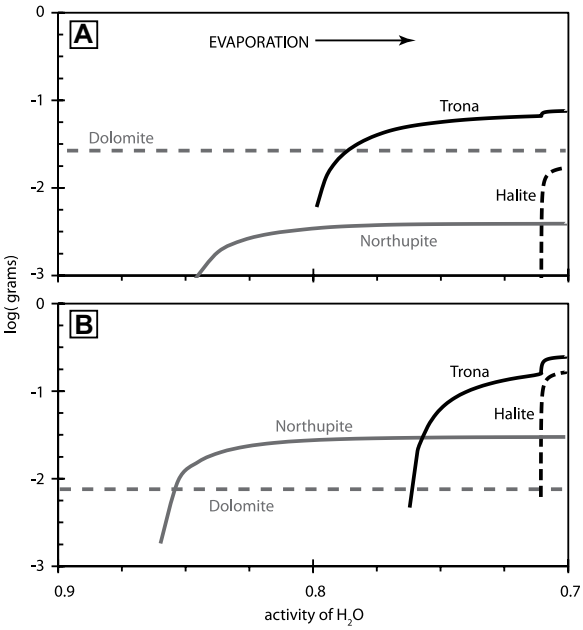

Figure 9. Selected mineral masses are shown as produced by (A) the complete evaporation of Owens River water at 23 °C, 200 ppm pCO_2 and (B) the complete evaporation of a hybrid solution created by stopping (A) at $aH_2O \approx 0.75$ and then diluting the brine with Owens River water by a factor of 1000.

produce a mixture with the same ionic ratios as fresh Owens River water. If the process of brine dilution is incomplete, and evaporation resumes prior to full dilution, then the subsequent evaporite mineralogy reflects the chemistry of the partially evaporated/diluted hybrid solution rather than Owens River water.

To assess the effects of partial evaporation/dilution on the mineral record, EQL/EVP was used to (1) evaporate Owens River water at 23 °C, 200 ppm pCO_2 to $aH_2O \approx 0.75$, and (2) dilute the brine with Owens River water by a factor of 1000 (e.g., 1000 kg Owens River water to 1 kg brine). Figure 9 compares the complete evaporation of standard Owens River water (Fig. 9A) to the partially evaporated/diluted hybrid water (Fig. 9B). Simulated evaporation/dilution alters brine composition as the components associated with less soluble salts are disproportionately removed by evaporation and insufficiently replenished by dilution. In contrast, components involved in the formation of the more soluble salts, such as Cl, are not removed during partial evaporation. As a result, dilution of the brine with Owens River water produces a hybrid brine enriched in more soluble components, which affects the mass of final precipitates (Figs. 9A–9B).

During evaporation of Owens River water, Mg^{2+} is nearly consumed during precipitation of dolomite, leaving later-formed northupite as a minor Mg-bearing mineral (Fig. 9A). This contrasts with the mineralogy of core SLAPP-SRLS17, in which northupite is the major Mg-bearing phase (Fig. 4). This discrepancy between the EQL/EVP and the SLAPP-SRLS17 mineralogy is rectified by partial evaporation/dilution cycles, where the lower initial concentrations of Ca^{2+} and Mg^{2+} in the hybrid water result in less dolomite precipitation, which in turn leaves excess Mg^{2+} in solution resulting in an increase in northupite precipitation (Fig. 9B). The occurrence of northupite as the dominant Mg-bearing mineral starting at the Bottom Mud/Lower Salt contact (Fig. 4B) indicates that partial evaporation/dilution cycles had already had a pronounced influence on Searles Lake chemistry by ca. 32 ka.

A more confounding discrepancy between the model simulations and the mineralogy of core SLAPP-SRLS17 is the relative mass abundances of trona and halite. Evaporation of Owens River water at 23 °C produces 4.4 times more trona than halite by mass (Fig. 9A). In contrast, trona/halite mass fractions for the Lower Salt and Upper Salt are 2.4 and 0.78, respectively (Table 3). The over-abundance of halite is apparent in Smith's (1976) mass-balance calculation for the Upper Salt, where he shows that the Owens River could only supply one-third of the Cl^- required to form the halite in the Upper Salt. Smith's mass-balance assumed that the Lower and Upper Salts were chemically distinct units, such that the ions that formed the evaporites in the Upper Salt were delivered to the basin during Parting Mud and Upper Salt deposition (24 k.y. of inflow). However, a long-term perennial Searles Lake would allow the Upper Salt to inherit excess Cl^- from the partial evaporation and dilution of older lakes.

Figure 9B shows the relative increase in the mass of halite if Searles Lake is evaporated to trona saturation and then diluted. The partial evaporation sequence results in a bed of trona and a Cl^-rich, HCO_3-CO_3-depleted brine. Dilution replenishes alkalinity and chlorinity at a 5:1 ratio, but the factor of dilution (1000) is insufficient to change the overall Alk/Cl^- ratio. As a result, the second evaporation sequence produces an evaporite unit with a trona/halite mass fraction of 1.5 (Fig. 9B). The inheritance of Cl^- from earlier lake phases via partial evaporation/dilution therefore explains the apparent halite anomalies reported by Smith (1976) and indicates that mass-balance calculations must be integrated at scales covering the complete dilution to complete evaporation of the lake rather than at arbitrary bed/unit scales (e.g., Parting Mud to Upper Salt). A revised mass balance (Table 4) shows that, assuming consistent solute chemistry and average discharge rates, ~112 k.y. of Owens River inflow is required to supply the chloride found within the Lower and Upper Salt, which suggests that the ions that formed the Lower and Upper Salts were partially derived from the remnants of the Marine Isotope Stage 6 lake.

TABLE 4. OWENS RIVER MASS BALANCE FOR THE UPPER AND LOWER SALT

Modern Owens River chemistry*		Annual solute flux§ ($\times 10^9$ g)	Searles bulk composition# ($\times 10^{12}$ g)			Required inflow for Upper and Lower Salt	
Component	(mg/L)		Upper Salt	Lower Salt	Total	($\times 10^{12}$ m^3)	($\times 10^3$ yr)
Na	31.9 ± 8.2	13.6	462	234	696	22	51
K	3.9 ± 0.8	1.7	28	9	37	9	22
Mg	4.0 ± 1.0	1.7	5	3	8	2	5
Total CO_3	99.7 ± 20.1	42.4	164	182	346	3	8
SO_4	22.6 ± 7.6	9.6	192	56	248	11	26
Cl	13.0 ± 4.2	5.5	448	171	619	48	112
B	0.77 ± N/A†	0.3	8	3	11	14	34
Ca	21.6 ± 4.1	9.2	–	–	–	–	–

*Mean values from 1974-1985 ± one standard deviation (Hollett et al., 1991).
†Smith (1976).
§Calculated using mean solute concentrations and mean annual Owens River discharge of 13.49 ± 5.66 m^3/s (Hollett et al., 1991).
#Smith (1979).

CONCLUSION

The chemical sediments of Pleistocene/Holocene Searles Lake display complex variability with respect to mineral phase, sequence, and mass that reflect various lake water conditions, such as temperature, pCO_2, salinity, water depth, hydrology, and long-term brine evolution. Thermodynamic modeling is demonstrated here as

Downloaded from http://pubs.geoscienceworld.org/gsa/gsabulletin/article-pdf/doi/10.1130/B35857.1/5242712/b35857.pdf
by SUNY Binghamton Science Library user

a powerful tool for deciphering complicated evaporite records in a way that provides valuable hydroclimatic insights and reconstructions.

Models for evaporating Owens River water produce all major minerals found in the Searles Lake deposit. The alkaline earth carbonates calcite, aragonite, and dolomite precipitate first as relatively freshwater precipitates. As lake water concentrates into a brine, the primary bedded evaporites are formed by *open* system fractional crystallization whereby chemical components are removed from the brine by salt precipitation and therefore drive subsequent brine evolution. Brine temperature and pCO_2 control the sequences and phases of *open* system evaporite precipitation. The defining evaporite sequence of core SLAPP-SRLS17 is trona → burkeite → halite, which indicates brine temperatures between 20 °C and 29 °C. Such consistent lake bottom water temperatures from 32 ka to 6 ka suggest stable lake depths >10 m during salt deposition. Anomalous phases, such as nahcolite instead of trona and thenardite in place of burkeite, suggest that Searles Lake, at times, experienced pulses of CO_2—likely fault-controlled injection—which increased lake water pCO_2 to ≥3 times atmospheric values.

Concurrent with primary *open* system precipitation, evolving lake brines also sink/diffuse along density gradients into underlying lake sediment. The resulting increase in pore-water salinity drives in situ, *closed* system back-reactions that replace laminated calcite and aragonite with gaylussite. Density diffusion appears to be limited by sediment compaction such that these back-reactions likely occur syndepositionally. Minerals formed in mud by back-reaction therefore reflect lake water temperatures and salinities and maintain approximate stratigraphic order with respect to the primary deposits. Pirssonite is therefore interpreted as a salinity-driven replacement of gaylussite and indicates hypersaline conditions.

Searles Lake was continuously perennial during the past 32–6 ka. Consequently, salt-mud stratigraphy does not represent cycles of flooding and subsequent desiccation but rather times of partial dilution of lake brine with Owens River water followed by times of partial evaporation. Cycles of partial dilution/evaporation explain "reverse" evaporite stratigraphy at the bed/unit scale and account for variability in mineral mass fractions as younger lakes inherit more soluble components, such as Cl, from older lakes. A model of long-term brine dynamics solves previous mass-balance anomalies by making Owens River inflow time an independent variable. The revised mass-balance calculation requires ca. 112 k.y. of inflow, which indicates that the Searles Lake evaporites deposited in the past 32–6 ka were partial remnants of the penultimate glacial lake (MIS 6) and that long-term brine evolution is a critical perspective for understanding saline lake systems and their corresponding deposits.

ACKNOWLEDGMENTS

The SLAPP-SRLS17 coring project would not be possible without the cooperation of Searles Valley Minerals Inc.; we give special thanks to Jade Brush. We thank our SLAPP-SRLS17 collaborators David McGee, Sarah Feakins, Joe Janick, Justin Stroup, Tripti Bhattacharya, Mark Peaple, Steve Lund, and Christine Chen for their valuable contributions and insights. Robert Demicco assisted with coding and provided suggestions that greatly improved an early draft of this manuscript. Logistical support during drilling and sample material used in this project provided by LacCore. This work was funded by the Comer Family Foundation and National Science Foundation Award 1903659, Paleo Perspectives on Climate Change Program, with additional support from the Geological Society of America, the American Association of Petroleum Geologists, and Society of Economic Geologists graduate student grants.

REFERENCES CITED

Barkan, E., Luz, B., and Lazar, B., 2001, Dynamics of the carbon dioxide system in the Dead Sea: Geochimica et Cosmochimica Acta, v. 65, no. 3, p. 355–368, https://doi.org/10.1016/S0016-7037(00)00540-8.

Bischoff, J.L., Rosenbauer, R.J., and Smith, G.I., 1985, Uranium-series dating of sediments from Searles Lake: Differences between continental and marine climate records: Science, v. 227, no. 4691, p. 1222–1224, https://doi.org/10.1126/science.227.4691.1222.

Cole, J.J., Caraco, N.F., Kling, G.W., and Kratz, T.K., 1994, Carbon dioxide supersaturation in the surface waters of lakes: Science, v. 265, no. 5178, p. 1568–1570, https://doi.org/10.1126/science.265.5178.1568.

De Cort, G., Mees, F., Renaut, R.W., Sinnesael, M., Van der Meeren, T., Goderis, S., Keppens, E., Mbuthia, A., and Verschuren, D., 2019, Late-Holocene sedimentation and sodium carbonate deposition in hypersaline, alkaline Nasikie Engida, southern Kenya Rift Valley: Journal of Paleolimnology, v. 62, p. 279–300, https://doi.org/10.1007/s10933-019-00092-2.

Demicco, R.V., and Lowenstein, T.K., 2020, When "evaporites" are not formed by evaporation: The role of temperature and pCO_2 on saline deposits of the Eocene Green River Formation, Colorado, USA: Geological Society of America Bulletin, v. 132, p. 1365–1380, https://doi.org/10.1130/B35303.1.

Du, Y., et al., 2019, Evaluation of boron isotopes in halite as an indicator of the salinity of Qarhan paleolake water in the eastern Qaidam Basin, western China: Geoscience Frontiers, v. 10, p. 253–262, https://doi.org/10.1016/j.gsf.2018.02.016.

Duarte, C.M., Prairie, Y.T., Montes, C., Cole, J.J., Striegl, R., Melack, J., and Downing, J.A., 2008, CO_2 emissions from saline lakes: A global estimate of a surprisingly large flux: Journal of Geophysical Research: Biogeosciences, v. 113, no. G04041, https://doi.org/10.1029/2007JG000637.

Eugster, H.P., and Smith, G.I., 1965, Mineral equilibria in the Searles Lake evaporites, California: Journal of Petrology, v. 6, p. 473–522, https://doi.org/10.1093/petrology/6.3.473.

Felmy, A.R., and Weare, J.H., 1986, The prediction of borate mineral equilibria in natural waters: Application to Searles Lake, California: Geochimica et Cosmochimica Acta, v. 50, no. 12, p. 2771–2783, https://doi.org/10.1016/0016-7037(86)90226-7.

Friedman, I., Smith, G.I., and Hardcastle, K., 1976, Studies of Quaternary saline lakes—II. Isotopic and compositional changes during desiccation of the brines in Owens lake, California, 1969–1971: Geochimica et Cosmochimica Acta, v. 40, no. 5, p. 501–511, https://doi.org/10.1016/0016-7037(76)90218-0.

Gale, H.S., 1914, Salines in the Owens, Searles, and Panamint Basins, Southeastern California: U.S. Geological Survey Bulletin 580-L, p. 251–323.

Hamdani, I., Assouline, S., Tanny, J., Lensky, I.M., Gertman, I., Mor, Z., and Lensky, N., 2018, Seasonal and diurnal evaporation from a deep hypersaline lake: The Dead Sea as a case study: Journal of Hydrology, v. 562, p. 155–167, https://doi.org/10.1016/j.jhydrol.2018.04.057.

Hardie, L.A., and Eugster, H.P., 1970, The evolution of closed-basin brines, *in* Morgan, B.A., ed., Fiftieth Anniversary Symposia: Mineralogy and Petrology of the Upper Mantle, Sulfides, Mineralogy and Geochemistry of Non-Marine Evaporites: Mineralogical Society of America Special Paper 3, p. 273–290.

Harvie, C.E., and Weare, J.H., 1980, The prediction of mineral solubilities in natural waters: The Na-K-Mg-Ca-Cl-SO_4-H_2O system from zero to high concentration at 25°C: Geochimica et Cosmochimica Acta, v. 44, no. 7, p. 981–997, https://doi.org/10.1016/0016-7037(80)90287-2.

Harvie, C.E., Møller, N., and Weare, J.H., 1984, The prediction of mineral solubilities in natural waters: The Na-K-Mg-Ca-H-Cl-SO_4-OH-HCO_3-CO_3-CO_2-H_2O system to high ionic strengths at 25°C: Geochimica et Cosmochimica Acta, v. 48, no. 4, p. 723–751, https://doi.org/10.1016/0016-7037(84)90098-X.

Hecht, A., and Gertman, I., 2003, Dead Sea meteorological climate, *in* Nevo, E., Oren, A., and Wasser, S.P., eds., Fungal Life in the Dead Sea: Liechtensein, Gantner, Ruggell, p. 68–114.

Hollett, K.J., Danskin, W.R., McCaffrey, W.F., and Walti, C.L., 1991, Geology and water resources of Owens Valley, California: U.S. Geological Survey Water-Supply Paper 2370–B, 77 p.

Jagniecki, E.A., Jenkins, D.M., Lowenstein, T.K., and Carroll, A.R., 2013, Experimental study of shortite ($Na_2Ca_2(CO_3)_3$) formation and application to the burial history of the Wilkins Peak Member, Green River Basin, Wyoming, USA: Geochimica et Cosmochimica Acta, v. 115, p. 31–45, https://doi.org/10.1016/j.gca.2013.04.005.

Jagniecki, E.A., Lowenstein, T.K., Jenkins, D.M., and Demicco, R.V., 2015, Eocene atmospheric CO_2 from the nahcolite proxy: Geology, v. 43, no. 12, p. 1075–1078, https://doi.org/10.1130/G36886.1.

Janick, J.J., and Demicco, R.V., 2019, Using a coupled geochemical/physical mass balance model to gain insights into the deposition of subrecent evaporites: Searles Valley, California, USA: Journal of Paleolimnology, v. 62, p. 105–120, https://doi.org/10.1007/s10933-019-00077-1.

Kiro, Y., Goldstein, S.L., Garcia-Veigas, J., Levy, E., Kushnir, Y., Stein, M., and Lazar, B., 2017, Relationships between lake-level changes and water and salt budgets in the Dead Sea during extreme aridities in the Eastern Mediterranean: Earth and Planetary Science Letters, v. 464, p. 211–226, https://doi.org/10.1016/j.epsl.2017.01.043.

Lee, H., Muirhead, J.D., Fischer, T.P., Ebinger, C.J., Kattenhorn, S.A., Sharp, Z.D., and Kianji, G., 2016, Massive and prolonged deep carbon emissions associated with continental rifting: Nature Geoscience, v. 9, p. 145–149, https://doi.org/10.1038/ngeo2622.

Lowenstein, T.K., and Demicco, R.V., 2006, Elevated Eocene atmospheric CO_2 and its subsequent decline: Science, v. 313, no. 5795, p. 1928–1928, https://doi.org/10.1126/science.1129555.

Lowenstein, T.K., Li, J., and Brown, C., 1998, Paleotemperatures from fluid inclusions in halite: Method verification and a 100,000 year paleotemperature record, Death Valley, CA: Chemical Geology, v. 150, p. 223–245, https://doi.org/10.1016/S0009-2541(98)00061-8.

Lowenstein, T.K., Li, J., Brown, C., Roberts, S.M., Ku, T.-L., Luo, S., and Yang, W., 1999, 200 ky paleoclimate record from Death Valley salt core: Geology, v. 27, p. 3–6, https://doi.org/10.1130/0091-7613(1999)027<0003:KYPRFD>2.3.CO;2.

Lowenstein, T.K., Dolginko, L.A., and García-Veigas, J., 2016, Influence of magmatic-hydrothermal activity on brine evolution in closed basins: Searles Lake,

Downloaded from http://pubs.geoscienceworld.org/gsa/gsabulletin/article-pdf/doi/10.1130/B35857.1/5242712/b35857.pdf
by SUNY Binghamton Science Library user

California: Geological Society of America Bulletin, v. 128, no. 9/10, p. 1555–1568, https://doi.org/10.1130/B31398.1.

Lowenstein, T.K., Jagniecki, E.A., Carroll, A.R., Smith, M.E., Renaut, R.W., and Owen, R.B., 2017, The Green River salt mystery: What was the source of the hyperalkaline lake waters?: Earth-Science Reviews, v. 173, p. 295–306, https://doi.org/10.1016/j.earscirev.2017.07.014.

Peterson, M.N.A., and Bien, G.S., 1966, Growth of dolomite crystals: American Journal of Science, v. 264, no. 4, p. 257–272, https://doi.org/10.2475/ajs.264.4.257.

Petit, J.R., et al., 1999, Climate and atmospheric history of the past 420,000 years from the Vostok ice core, Antarctica: Nature, v. 399, no. 6735, p. 429, https://doi.org/10.1038/20859.

Pitzer, K.S., 1973, Thermodynamics of electrolytes. I. Theoretical basis and general equations: Journal of Physical Chemistry, v. 77, p. 268–277, https://doi.org/10.1021/j100621a026.

Pretti, V.A., and Stewart, B.W., 2002, Solute sources and chemical weathering in the Owens Lake watershed, eastern California: Water Resources Research, v. 38, no. 8, p. 2-1–2-18, https://doi.org/10.1029/2001WR000370.

Renaut, R.W., Owen, R.B., Lowenstein, T.K., De Cort, G., McNulty, E., Scott, J.J., and Mbuthia, A., 2020, The role of hydrothermal fluids in sedimentation in saline alkaline lakes: Evidence from Nasikie Engida, Kenya Rift Valley: Sedimentology, https://doi.org/10.1111/SED.12778, (in press).

Risacher, F., and Clement, A., 2001, A computer program for the simulation of evaporation of natural waters to high concentration: Computers & Geosciences, v. 27, p. 191–201, https://doi.org/10.1016/S0098-3004(00)00100-X.

Roberts, S.M., and Spencer, R.J., 1995, Paleotemperatures preserved in fluid inclusions in halite: Geochimica et Cosmochimica Acta, v. 59, no. 19, p. 3929–3942, https://doi.org/10.1016/0016-7037(95)00253-V.

Rosenthal, J.S., Meyer, J., Palacios-Fest, M.R., Young, D.C., Ugan, A., Byrd, B.F., Gobalet, K., and Giacomo, J., 2017, Paleohydrology of China Lake basin and the context of early human occupation in the northwestern Mojave Desert, USA: Quaternary Science Reviews, v. 167, p. 112–139, https://doi.org/10.1016/j.quascirev.2017.04.023.

Ross, Z.E., et al., 2019, Hierarchical interlocked orthogonal faulting in the 2019 Ridgecrest earthquake sequence: Science, v. 366, no. 6463, p. 346–351, https://doi.org/10.1126/science.aaz0109.

Sirota, I., Enzel, Y., and Lensky, N.G., 2017, Temperature seasonality control on modern halite layers in the Dead Sea: In situ observations: Geological Society of America Bulletin, v. 129, no. 9/10, p. 1181–1194, https://doi.org/10.1130/B31661.1.

Smith, G.I., 1962, Subsurface stratigraphy of late Quaternary deposits, Searles Lake, California—A summary; *in* Geological Survey Research 1962: U.S. Geological Survey Professional Paper 450–C, p. C65–C69.

Smith, G.I., 1976, Origin of lithium and other components in the Searles Lake evaporites, California, *in* Vine, J.D., ed., Lithium Resources and Requirements by the Year 2000: U.S. Geological Survey Professional Paper 1005, p. 92–103.

Smith, G.I., 1979, Subsurface stratigraphy and geochemistry of late Quaternary evaporites, Searles Lake, California: U.S. Geological Survey Professional Paper 1043, 130 p.

Smith, G.I., Barczak, V.J., Moulton, G.F., and Liddicoat, J.C., 1983, Core KM-3, a surface-to-bedrock record of Late Cenozoic sedimentation in Searles Valley, California: Geological Survey Professional Paper, v. 1256, p. 29, https://doi.org/10.3133/pp1256.

Smith, G.I., 2009, Late Cenozoic geology and lacustrine history of Searles Valley, Inyo and San Bernardino Counties, California: U.S. Geological Survey Professional Paper 1727, p. 128, https://doi.org/10.3133/pp1727.

Smith, G.I., and Haines, D.V., 1964, Character and distribution of nonclastic minerals in the Searles Lake evaporite deposit, California: U.S. Geological Survey Bulletin 1181–P, 58 p.

Smith, G.I., Friedman, I., and McLaughlin, R.J., 1987, Studies of Quaternary saline lakes—III. Mineral, chemical, and isotopic evidence of salt solution and crystallization processes in Owens Lake, California, 1969–1971: Geochimica et Cosmochimica Acta, v. 51, p. 811–827, https://doi.org/10.1016/0016-7037(87)90095-0.

Sorey, M.L., 1985, Evolution and present state of the hydrothermal system in Long Valley Caldera: Journal of Geophysical Research. Solid Earth, v. 90, no. B13, p. 11219–11228, https://doi.org/10.1029/JB090iB13p11219.

Spencer, R.J., Eugster, H.P., and Jones, B.F., 1985, Geochemistry of Great Salt Lake, Utah II: Pleistocene-Holocene evolution: Geochimica et Cosmochimica Acta, v. 49, no. 3, p. 739–747, https://doi.org/10.1016/0016-7037(85)90168-1.

Stuiver, M., and Smith, G.I., 1979, Radiocarbon ages of stratigraphic units, *in* Smith, G.I., ed., Subsurface Stratigraphy and Geochemistry of Late Quaternary Evaporites, Searles Lake, California: U.S. Geological Survey Professional Paper 1043, p. 68–75.

Teeple, J.E., 1929, Industrial Development of Searles Lake Brines, with Equilibrium Data: New York, American Chemical Society Monograph Series, no. 49, 182 p.

Wang, N., Li, Z., Li, Y., Cheng, H., and Huang, R., 2012, Younger Dryas event recorded by the mirabilite deposition in Huahai lake, Hexi Corridor, NW China: Quaternary International, v. 250, p. 93–99, https://doi.org/10.1016/j.quaint.2010.11.017.

Wanninkhof, R., and Knox, M., 1996, Chemical enhancement of CO_2 exchange in natural waters: Limnology and Oceanography, v. 41, no. 4, p. 689–697, https://doi.org/10.4319/lo.1996.41.4.0689.

Wurtsbaugh, W.A., and Berry, T.S., 1990, Cascading effects of decreased salinity on the plankton chemistry, and physics of the Great Salt Lake (Utah): Canadian Journal of Fisheries and Aquatic Sciences, v. 47, no. 1, p. 100–109, https://doi.org/10.1139/f90-010.

Science Editor: Wenjiao Xiao
Associate Editor: Ganqing Jiang

Manuscript Received 3 August 2020
Revised Manuscript Received 20 November 2020
Manuscript Accepted 9 January 2021

Printed in the USA

Downloaded from http://pubs.geoscienceworld.org/gsa/gsabulletin/article-pdf/doi/10.1130/B35857.1/5242712/b35857.pdf
by SUNY Binghamton Science Library user